Activation mechanisms of the scramblase Xkr4

ZHANG Panpan

Contents

Abstract

Phosphatidylserine is exposed on the cell surface of dying cells as an “eat me” signal by phospholipid scrambling (PLS), which is regulated by membrane proteins called scramblases. In previous studies, we found that the scramblase Xkr4 dimer was activated in the presence of the caspases-generated fragment of XRCC4 (XRCC4/C). However, it remains unknown how Xkr4 is activated in dying cells. In this study, I aimed to understand the activation mechanisms of Xkr4. Applying a protein-protein interaction screening, I demonstrated that XRCC4/C activated Xkr4 dimer through direct binding. During these analyses, I noticed that caspase-activated Xkr4 cannot induce PLS when the extracellular divalent cations are removed. Constitutively-active mutant of Xkr4 (aXkr4) in living cells also required the divalent cations to induce PLS. Through metal ions screening, I found that the metal ions including Ca^{2+}, Sr^{2+}, Mn^{2+}, or Tb^{3+} are the additional factors associated with the aXkr4-mediated PLS activity. Among these ions, Ca^{2+} activates Xkr4 with the highest affinity. I also found that other Xkr family members, Xkr8 and Xkr9, required Ca^{2+} for activation. To identify the potential Ca^{2+}-binding site, Xkr4, Xkr8, and Xkr9 were aligned. Unexpectedly, the conserved negatively-charged amino acids generated a Ca^{2+}-binding pocket in the transmembrane (TM) regions. The alanine mutations confirmed that the extracellular Ca^{2+} interacts with D123 and D127 of TM1 and E310 of TM3, where Ca^{2+} functions as a molecular glue to connect TM1 and TM3. To prove the effect of Ca^{2+} to connect TM1 and TM3, cysteine mutations were introduced into the Ca^{2+}-binding sites, by which the artificial disulfide bond is formed. As a result, E310C/G125C double mutations facilitated PLS without extracellular Ca^{2+}. Furthermore, lysine mutations were introduced to generate a salt bridge. As a result, E310K mutation activated aXkr4 without the extracellular Ca^{2+}. These results strongly demonstrated that Ca^{2+} functions as molecular glue to connect TM1 and TM3 for Xkr4 activation. In summary, I revealed that Xkr4 activation requires direct binding of the XRCC4 fragment and the extracellular Ca^{2+}, thus demonstrating that the sophisticated interplay of extracellular and nuclear molecules regulate phospholipid scrambling on the plasma membranes.

Abbreviation

ACN	Acetonitrile
AGC	Automatic gain control
aXkr4	Activated mutant mXkr4ΔC
ATP	Adenosine Triphosphate
BDKO	A deficient in TMEM16F and Xkr8 of Ba/F3 cells
BN-PAGE	Blue Native-PAGE
BSG	Basigin
Casp3	Caspase3
CBB	Coomassie brilliant blue
CD	C-terminal domain
cDNA	Complementary DNA
cEK	Enterokinase catalytic subunit
CHES	N-cyclohexyl-2-aminoethanesulfonic acid
CMC	Critical micelle concentration
CuP	Copper-phenanthroline
DNA	Deoxyribonucleic acid
ER	Endoplasmic reticulm
EK	Enterokinase
FACS	Fluorescence-activated cell sorting
FBS	Fetal bovine serum
FS293F	Freestyle 293F
GDN	Glyco-dendrimer
GFP	Green fluorescence protein
GLs	Glycerophospholipids
GSH	Glutathione
GSSG	Glutathione disulfide
HBSS	Hanks' Balanced Salt Solution
HEPES	4-(2-hydroxyethyl)-1-piperazineethanesulfonic acid
hXkr4ΔC	Human Xkr4 without C-terminus
HPLC	High Performance Liquid Chromatography
IDR	Intrinsically disordered region
IL-3	Interleukin 3
IP	Immunoprecipitation
IPTG	Isopropyl β-D-1-thiogalactopyranoside
ISP	Insulin signal peptide
LB	Lysogeny broth
LMNG	Lauryl Maltose Neopentyl Glycol
LC-MS/MS	Liquid Chromatograph – Mass Spectrometry
LigIV	DNA ligaseIV
MD	Molecular dynamics
mEGFP	Monomeric enhance GFP
MOI	Multiplicity of infection
MS	Mass Spectrometry
mXkr4FL	Mouse Xkr4 full length
NBD-PC	7-nitrobenz-2-oxa-1,3-diazol-4-yl phosphatidylcholine
NBD-SM	7-nitrobenz-2-oxa-1,3-diazol-4-yl -sphingomyelin

NCD	N-terminal cytosolic domain
NPTN	Neuroplastin
P4-ATPase	Type IV P-type ATPases
PC	Phosphatidylcholine
PDVF	Polyvinylidene difluoride
PE	Phosphatidylethanolamine
PEI	Polyethylenimine
PI	Phosphatidylinositol
PLS	Phospholipid scramblase
PMs	Plasma membranes
PS	Phosphatidylserine
RFU	Relative fluorescence unit
RNA	Ribonucleic acid
RT	Room temperature
SDS	Sodium Dodecyl Sulfate
SEC	Size exclusion chromatography
sgRNA	Short guide RNA
SM	Sphingolipids
SMA	Stryrene-maleic acid mediate nanodisc
STS	Staurosporine
STs	Sterols
TB	Terrific Broth
Thapsi	Thapsigargin
TM	Transmembrane
UHPLC	Ultra High-Performance Liquid Chromatography
UV	Ultraviolet
Xkr4ΔC	Mouse Xkr4 without C-terminus
XRCC4/C	C-terminus of XRCC4

1. Introduction

1.1 Phosphatidylserine exposure on cell surface

Cell plasma membranes (PMs) serve as a vital functional barrier separating the cells from the surrounding environment to maintain the essential physiological processes. The core of PMs composes a diversity of lipid species which can be mainly classified into three categories based on their backbone structure: glycerophospholipids (GLs), sphingolipids (SM), and sterols (STs)[1]. The GLs is one of the major components that comprises a hydrophobic tail (acyl chains), glycerol backbone, and hydrophilic head group. According to their distinct head groups, GPs are divided into phosphatidylethanolamine (PE), phosphatidylinositol (PI), phosphatidylserine (PS), phosphatidylcholine (PC), and phosphatidic acids. In rat liver PMs, PC constitutes approximately 43% of total phospholipids, PE does 21%, and SM does 23%. Meanwhile, the amount of PI and PS is lower, accounting for approximately 7% and 4%, respectively[2].

In eukaryote cells, phospholipids in PMs are distributed in an asymmetrical manner: PC and SM are mainly concentrated in the outer leaflet, while PS and PE are concentrated in the inner leaflet of the membranes[3,4]. To maintain the asymmetrical distribution of the phospholipids in living cells, Type IV P-type ATPases (P4-ATPase) function as a flippase using ATP as an energy and translocate PE and PS from the outer lipid bilayer into the inner bilayer against the concentration gradient of lipid molecules[5] (Fig. 1). However, this asymmetrical distribution of phospholipids can be dynamically changed, allowing cells to respond to various physiological situations and adapt to the acute environmental changes. In particular, PS exposure on the cell surface has been known to function as critical signals or scaffolds to communicate with extracellular environments. For instance, PS exposure on the activated platelet serves as a scaffold for coagulation factors to initiate the clotting reaction when endothelial cells suffer injury[6]. During apoptosis, PS functions as an “eat me” signal for unwanted cells to be engulfed by phagocytes. When apoptotic cells are not engulfed by phagocytes, they become burst and release the intracellular molecules including DNA, RNA, and proteins, and lead to inflammation. To prevent such inflammation, PS is exposed on the cell surface of unwanted cells to be swiftly engulfed by neighboring phagocytes[7,8].

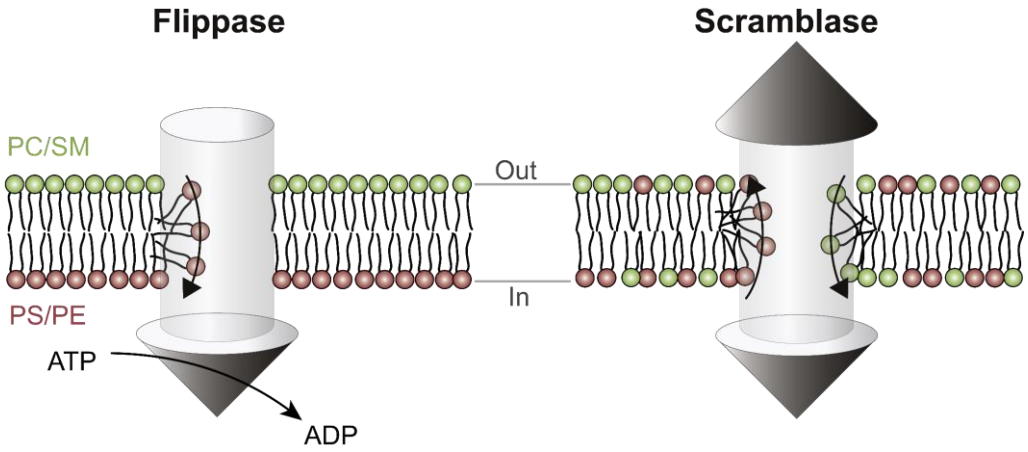

Fig. 1: Models of Flippase and Scramblase Flippase transfer phospholipid (PS/PE) from outer lipid bilayer to inner lipid bilayer using ATP as energy (left). Scramblase transfer lipids including PS, PE, PC and SM to both lipid bilayer (right).

To rapidly expose PS to the cell surface, membrane proteins, called scramblases, that transport phospholipids bidirectionally and non-specifically (this process is also called as phospholipid scrambling (PLS)) need to be activated[9–11]. Currently, two family members of scramblases have been identified by Suzuki and colleagues: the calcium-dependent scramblase TMEM16 family and the caspase-dependent scramblase Xkr family[12–15] (Fig.1).

1.2 Lipid scrambling by TMEM16 family

1.2.1 Scramblase in TMEM16 family

In 2010, TMEM16F was identified as a long-sought after Ca^{2+}-dependent scramblase on plasma membranes through the cDNA library screening approach[14]. Subsequent studies proved that TMEM16F is a catalytic subunit of scramblases by reconstituting it into the liposome or a multi-channel membrane system using purified proteins[16,17]. Through the calculation, a scramblase was found to transfer nearly 4.5×10^4 lipids per second[17]. TMEM16F belongs to the TMEM16 family, consisting of 10 members, all of which have 10 transmembrane helices. Initially, TMEM16 family has been believed to function as an ion channel because TMEM16A and TMEM16B were identified and characterized as a chloride (anion) channel[18–20]. However, the subsequent studies suggested that most of the TMEM16 family members function as a scramblase. In TMEM16F family, there are ten members, and five of them, TMEM16C, 16D, 16F, 16G, and 16J, exhibit a PLS activity on PMs and two of them, 16E and 16K, do at intracellular membranes[13,21]. TMEM16F is ubiquitously expressed in tissues, while other family proteins show a tissue-specific expression: 16C is expressed in the brain,

16D is expressed in the uterus and ovary, 16E is expressed in skeletal muscle, 16G is expressed in the stomach and prostate, and 16J is expressed in the intestine[22,23].

1.2.1 Activation of TMEM16 by Ca^{2+} binding

Although TMEM16 family proteins show different functions such as ion channels and scrambles, a highly conserved activation mechanism is shared through the family members. To activate TMEM16 family proteins, two steps are required: 1. Two TMEM16 monomer form a homodimer; 2. The intracellular Ca^{2+} directly binds to the TMEM16 proteins to induce the conformational changes. Based on the analyzed structure of TMEM16 family proteins including TMEM16A[24], TMEM16F[25], TMEM16K[26], and afTMEM16[27], nhTMEM16[28,29], all of them showed a homodimer, in which each monomer consists of 10 transmembrane helices, a long N-terminal cytosolic domain (NCD), a short C-terminal domain (CD), and two Ca^{2+}-binding sites (Fig. 2).

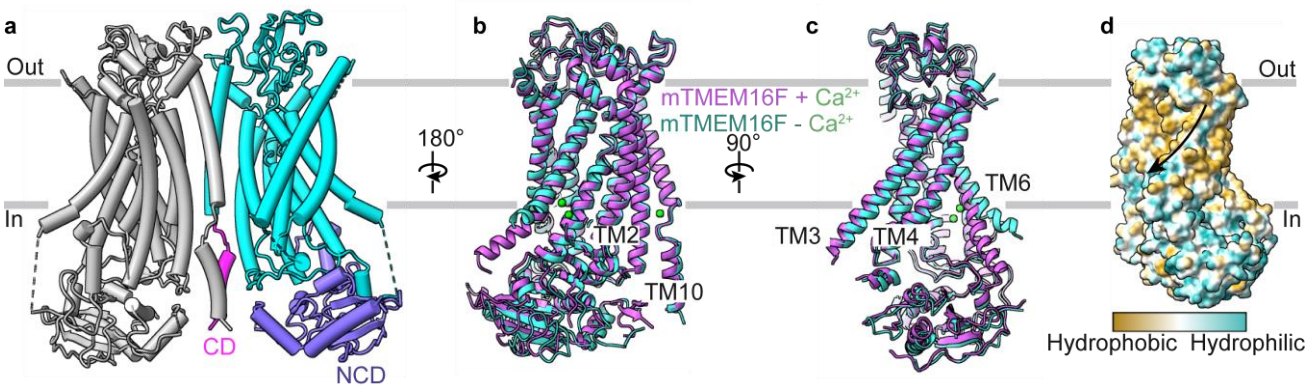

Fig. 2: Structure of TMEM16F a mouse TMEM16F (mTMEM16F) dimer structure (PDB: 6QPB), Blue: N-terminal cytosolic domain (NCD) of TMEM16F; Pink: The C-terminus domain (CD) of TMEM16F. Dark Turquoise: The transmembrane domain of TMEM16F. **b**, **c** View of comparation of mTMEM16 without (Dark turquoise; PDB: 6QPB) and with Ca^{2+} (Dark violet; PDB: 6QP6). The bound Ca^{2+} ions are represented as greed spheres. **d** The hydrophobicity of surface with mTMEM16F with Ca^{2+}, orange represents the hydrophobic and light blue represents the hydrophilic. The lipid transfer pathway was highlight by a black arrow.

To activate TMEM16 family proteins, two Ca^{2+} need to access from the intracellular side and directly bind to the TM6, TM7, and TM8 to induce the conformational change. In addition, an extra Ca^{2+} binds to the TM2 and TM10 (Fig. 2b), but how the Ca^{2+} binding to TM2 and TM10 regulates the TMEM16 proteins is still unclear[26,30]. Based on the structural analysis, mechanisms of PLS have been well characterized: a hydrophilic cavity, consisting of polar residues, is formed in the protein surface toward lipids, enabling the phospholipid head to pass through. Generally, these polar residues are hidden inside the protein under the resting condition but exposed on the surface to generate the cavity when

the scramblases are activated. The lipid transfer pathway is composed of TM3 to TM7. When two Ca^{2+} bind to the TM6, TM7, and TM8, a conformational change is induced especially on the TM6, which swings and indues the rearrangements of other transmembrane regions (Fig. 2c). As a result, the hydrophilic lipid transfer pathway is exposed to lipid surface so that phospholipid head can pass through the protein surface (Fig. 2d)[31]. This process is also known as a "credit card" model[11], in which the phospholipid heads are permeated through the hydrophilic cavity, while the acyl chains remain in the lipid layer during lipid translocation. This model has been supported by other studies using MD simulation[16,32]. Not only changes in the protein conformation, but also the changes in lipid bilayer can be observed: the bilayer got distorted and thinner when afTMEM16 and TMEM16F structures were analyzed in nanodisc[31,33,34].

1.3 Lipid scrambling by Xkr family

1.3.1 Scramblase in Xkr family

In contrast to a Ca^{2+}-dependent scramblase, TMEM16 family, Xkr family are caspase-dependent scramblase which has a caspase-cleavage site at the C-terminus. Some of them mainly function for the clearance of dead cells by exposing PS to the outer layer of the membrane[13,15]. In the mouse Xkr family, there are eight family members including Xkr1 (or Xk), Xkr2, Xkr4, Xkr5, Xkr6, Xkr7, Xkr8, and Xkr9. Among these members, four of them, Xkr1, Xkr4, Xkr8, and Xkr9 have been identified as a scramblase. Xkr4 and Xkr9 are tissue-specifically expressed in the brain and small intestine, respectively. In contrast, Xkr8 is ubiquitously expressed in tissues[13].

1.3.2 Activation mechanism of Xkr family

Similar to the TMEM16 family, Xkr family proteins are activated by forming a homodimer after the cleavage at the C-terminus by caspase[13,35]. In 2021, two groups revealed the monomer structure of mouse Xkr8 and rat Xkr9[36,37]. Based on the structural analysis, a highly conserved structure was shown in the Xkr family proteins: 8 transmembrane helices and 2 intermedia transmembrane helices (IH) between the TM2 and TM3, and TM6 and TM7[36,37]. In the case of Xkr9, structures of the full-length protein and truncated one, deleted in the C-terminus, were analyzed and compared. The results showed that the C-terminus of Xkr9 binds to the hydrophobic pocket formed by the TM3 to TM5, TM8, and IH2[36], suggesting that the C-terminus stabilizes the inactive conformation of Xkr family proteins. However, it is unknown how the cleavage of C-terminus facilitates the dimer formation[13,23,35]. Using

the liposome analysis, reconstitution of Xkr9 monomer either in full length or cleaved form was performed, but no PLS activity was shown, suggesting that the dimer formation is required to activate Xkr9[36]. Interestingly, because dimer formation is not enough for some Xkr family members[13], additional factors might be required to activate Xkr family members.

Xkr4 is highly expressed in brain[13]. To identify the activating factors for Xkr4, we performed a reviving screening by using the sgRNA library in PLB cells where the DNase *CAD* was knocked out to prevent the genomic DNA from degradation after inducing the cell death[38]. Surprisingly, the nuclear localization protein XRCC4 was found to regulate Xkr4 activation[39]. In general, XRCC4 is known to regulate the DNA repair by forming a complex with XLF and DNA Ligase IV in the nucleus[40,41]. However, the C-terminus of XRCC4 was cleaved in the nucleus by caspase 3 during apoptosis, followed by release of the cleaved fragment from the nucleus into the cytosol (Fig. 3). In that study, we also identified the minimum region of XRCC4 C-terminus (XRCC4/C) for activation of Xkr4, which corresponds to the region from amino acids (a.a.) 266 to 286[39]. However, XRCC4/C is not necessary for activation of Xkr8 and Xkr9, suggesting that each Xkr family member has the different activation mechanisms.

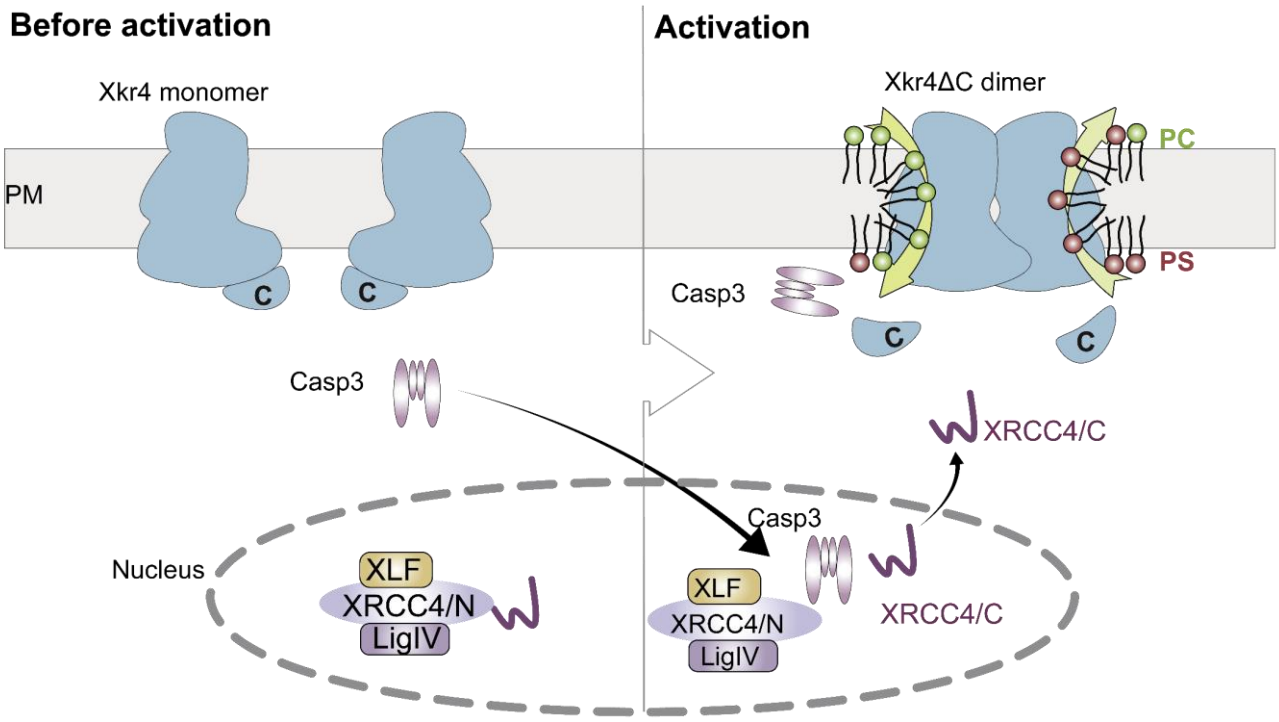

Fig. 3: Activation model of Xkr4 The activation model of Xkr4. The C-terminus of Xkr4 was cleaved by caspase3 (Casp3), and form a homodimer in plasma membrane. The C-terminus of XRCC4 (XRCC4/C) was cleaved by Casp3 in nucleus and released into cytosol to activation Xkr4. LigIV,

DNA ligaseIV.

1.3.3 Chaperons of Xkr family

Most of Xkr family members localize on the plasma membrane. In the case of Xkr8, Basigin (BSG) and Neuroplastin (NPTN) were identified as chaperons, one of which is necessary to form a heterodimer with Xkr8 so that Xkr8 can localize on the plasma membrane. After the caspase cleavage at C-terminus, Xkr8 forms a heterotetramer[35] (Fig. 4). However, binding with BSG or NPTN was not necessary for other Xkr family members. Xkr1 is a paralogue of Xkr8 and forms a complex with the cytoplasmic lipid transporter Vps13a, connecting the ER and plasma membrane. Xkr1 functions as a scramblase exposing PS on T cell surface in response to ATP stimulation[42,43]. However, it remains an open question whether other Xkr family members require chaperons for their functions.

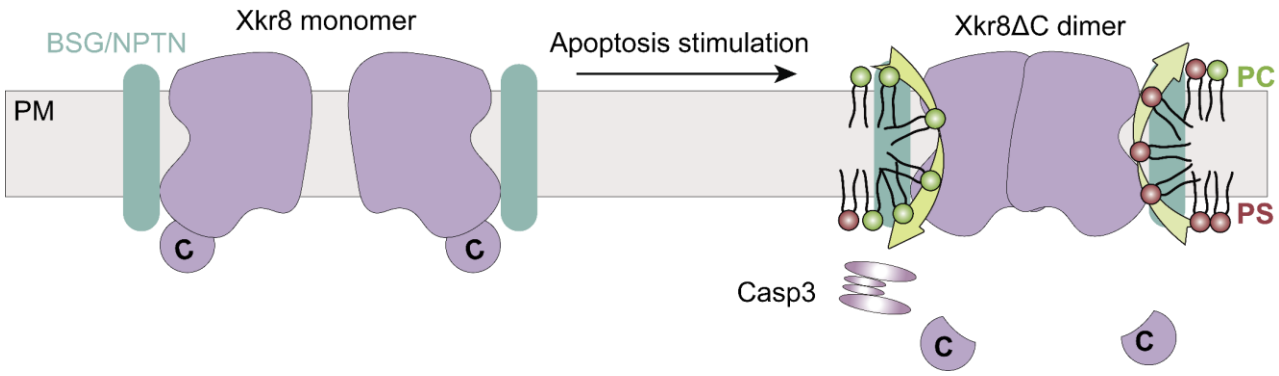

Fig. 4: Activation model of Xkr8 BSG or NPTN binds to Xkr8 in plasma membrane at a ratio of 1:1. The C-terminus of Xkr8 was cleaved by caspase3 (Casp3) during apoptosis and form a homotetramer in plasma membrane as a activate formation. BSG, Basigin. NPTN, Neuroplastin.

1.4 Project aim and summary

Compared to widely-studied TMEM16 family, Xkr family is not studied well. At least, we know that some of Xkr family members expose PS as an “eat me” signal on the cell surface. Expose PS has been known to play critical roles in the clearance of the dead cells, synapse elimination, and removal of nucleus during enucleation[23,39,44]. However, it is not completely understood how Xkr proteins are activated. In this project, I am focusing on understanding the activation mechanisms of Xkr4.

I especially try to answer 2 questions: 1. How does XRCC4/C regulate Xkr4? 2. What are the additional regulators to activate Xkr4? To answer the first question, I performed a protein-protein interaction

screening, combining immunoprecipitation (IP) and mass spectrometry. Xkr4 was tagged with a SPOT tag and expressed in Xkr4 dimer-expressing cells, followed by immunoprecipitation of Xkr4 interactors and mass spectrometry. The results showed that XRCC4/C activated Xkr4 in a direct binding manner. To identify the other missing factors for activation of Xkr4, a metal ion screening was performed. As a result we found that the extracellular Ca^{2+} is required to activate Xkr4. Unexpectedly, the extracellular Ca^{2+} accesses from the extracellular side and binds to D123, D127 of TM1 and E310 of TM3. Furthermore, T307 and S311 of TM3, and S342 of TM4 also support the Ca^{2+} binding. Basing on these results, we hypothesized that the extracellular Ca^{2+} functions as a "molecular glue" to connect the TM1 and TM3. Using the Cys scanning to introduce an artificial disulfide bond and Lys scanning to introduce an artificial salt bridge in Ca^{2+} binding sites, I demonstrated that Ca^{2+} functions as molecular glue to bridge the TM1 and TM3 to induce the conformational change and activate Xkr4.

2. Material and methods

2.1 List of Plasmids and reagents

REAGENT or RESOURCE	SOURCE	IDENTIFIER
Antibodies		
anti-V5-HRP	Thermo Fisher Scientific	Cat# R961-25
anti-mouse basigin	Biolegend	Cat# 123701
anti-rat IgG biotin	Thermo Fisher Scientific	Cat# 31830
ploryclonal goat anti-rabbit immunoglobulins/HRP	DAKO	Cat# P0488
Anti tagRFP	Evrogen	Cat# AB23
Chemicals		
NBD-PC	Avanti Polar Lipids	810132p
BSA Fatty-acid free	Sigma-aldrich	A6003
Staurosporine	LC laboratories	S-9300
DAPI	Dojindo	D523 CAS: 28718-90-3
copper-phenanthrolin	Tokyo Chemical Industry	D3891
Iodine solution	Fujifilm	099-00471
GDN	Anatrace	GDN101
Digitonin	Wako	043-21371
Lauryl Maltose Neopentyl Glycol (LMNG)	Anatrace	NG310
Experimental Models: Cell Lines		
293T cells	Pear et al., 1993	S. Nagata lab, Osaka Univ.
FreeStyle 293F cells	This paper	K. Takuya Lab, Kyoto Univ.
BDKO cells (Ba/F3 cells deficient for Xkr8 and TMEM16F)	This paper	N/A
PLB cells deficient for XRCC4 and CAD	This paper	N/A
BL21(DE3)	NEW ENGLAND BioLabs	C2527H
Recombinant DNA		
plenti-IERS-Puro	Maruoka et al., 2021[39]	N/A
pEGBacMam-V5-human-Xkr4ΔC-FLAG-mEGFP-His_{10}	This paper	K. Takuya Lab, Kyoto Univ.
pCold1 XRCC4-His_8	This paper	N/A
pGEX-5X-1 XRCC4/C-His_8	This paper	N/A
pGEX-5X-1 XRCC4/C I266G-His_8	This paper	N/A
pCEX-5X-1 XRCC4/C R270A-His_8	This paper	N/A
pGEX-5X-1 cEK	This paper	N/A
pNEF V5-mouse Xkr4ΔC-FLAG-monomeric EGFP	This paper	N/A

pMXs-puro V5-mouse Xkr4FL-FLAG	This paper	N/A
pMXs-puro V5-mouse Xkr4ΔC-FLAG	This paper	N/A
plenti V5-human Xkr4-IRES-Puro	Maruoka et al., 2021[39]	N/A
plenti V5-human Xkr8-IRES-Puro	Maruoka et al., 2021[39]	N/A
plenti V5-human Xkr9-IRES-Puro	Maruoa et al., 2021[39]	N/A
plenti V5-mouse Xkr8-IRES-Puro	This paper	N/A
plenti V5-mouse Xkr9-IRES-Puro	This paper	N/A
pMXs V5-mouse Xkr4ΔC Q332E-FLAG-tagRFP	This paper	N/A
pMXs V5-mouse Xkr4ΔC D123A/Q332E-FLAG-tagRFP	This paper	N/A
pMXs V5-mouse Xkr4ΔC D127A/Q332E-FLAG-tagRFP	This paper	N/A
pMXs V5-mouse Xkr4ΔC E310A/Q332E-FLAG-tagRFP	This paper	N/A
pMXs V5-mouse Xkr4ΔC D123N/Q332E-FLAG-tagRFP	This paper	N/A
pMXs V5-mouse Xkr4ΔC D127N/Q332E-FLAG-tagRFP	This paper	N/A
pMXs V5-mouse Xkr4ΔC E310N/Q332E-FLAG-tagRFP	This paper	N/A
pMXs V5-mouse Xkr4ΔC D123C/Q332E-FLAG-tagRFP	This paper	N/A
pMXs V5-mouse Xkr4ΔC V124C/Q332E-FLAG-tagRFP	This paper	N/A
pMXs V5-mouse Xkr4ΔC G125C/Q332E-FLAG-tagRFP	This paper	N/A
pMXs V5-mouse Xkr4ΔC T126C/Q332E-FLAG-tagRFP	This paper	N/A
pMXs V5-mouse Xkr4ΔC E310C/Q332E-FLAG-tagRFP	This paper	N/A
pMXs V5-mouse Xkr4ΔC D123C/E310C/Q332E-FLAG-tagRFP	This paper	N/A
pMXs V5-mouse Xkr4ΔC V124C/E310C/Q332E-FLAG-tagRFP	This paper	N/A
pMXs V5-mouse Xkr4ΔC G125C/E310C/Q332E-FLAG-tagRFP	This paper	N/A
pMXs V5-mouse Xkr4ΔC T126C/E310C/Q332E-FLAG-tagRFP	This paper	N/A
pMXs V5-mouse Xkr4ΔC D127C/E310C/Q332E-FLAG-tagRFP	This paper	N/A
Software and Algorithms		
ImageJ	Schneider et al., 2012[45]	https://imagej.nih.gov/ij/
GraphPad PRISM 9.2.0	GraphPad	https://www.graphpad.com
Illustrator V 26.0.3	Adobe Illustration	https://www.adobe.com/products/illustrator.html

FlowJo	FlowJo.LLC	https://www.flowjo.com/
Chimera 1.16	UCSF chimera program	https://www.cgl.ucsf.edu/chimera/
Chimera X 1.4	UCSF chimera program	https://www.rbvi.ucsf.edu/chimerax/
Jalview 2.11.1.7	Waterhouse et.al., 2009[46]	https://www.jalview.org/
Matplotlib 3.5.1	Hunter, J,D 2007 [47]	https://matplotlib.org/
Numpy	Harries et al., 2020[48]	https://numpy.org/
Modeller 10.1	Sánchez, R et al., 1997[49]	https://salilab.org/modeller/
Other		
Robetta: structure prediction	Baek et al., 2021[50]	https://robetta.bakerlab.org/submit.php
Streptavidin conjugated beads	SPHERO™	SVP-15-5
Hiload 26/600 superdex75 pg	GE healthcare	Cytiva 28-9893-34
Glutathione Sepharose 4B	GE healthcare	Cytiva 17-0756-04
Ni-NTA agarose HP	Fujifilm	141-09683
Fluorescence Size exclusion chromatography	Shimadzu	N/A

2.2 Cell lines

FreeStyle 293-F cells were cultured in FreeStyle 293 Expression medium (Gibco) with supplements of 2 % FBS (Gibco) at 120 rpm, 37 ℃, and 8% CO_2. Insect cell sf9 was cultured in PSFM-JI Medium (Wako) containing 2% FBS at 120 rpm, 27 ℃. HEK293T cells were cultured in Dulbecco's modified Eagle's medium (WAKO) with supplements of antibiotics (Nacalai) and 10% FBS (Gibco). Mouse interleukin 3 (IL-3)-dependent Ba/F3 cells[51] were cultured in RPMI1640 (WAKO) with supplements of 55 μM β-mercaptoethanol, 45 units/ml IL-3[52], 10% FBS, and antibiotics, Human PLB985 cells (hereafter PLB)[53] were cultured in RPMI1640 with supplements of 55 μM β-mercaptoethanol, 10% FBS, and antibiotics. ALL HEK293T cells, Ba/F3 cells and PLB985 cells were cultured at 37 ℃ and 5 % CO_2.

2.3 Construction of plasmids

Mouse (m) Xkr4 full-length (mXkr4FL), or Xkr4ΔC which C-terminus was removed were cloned into the pMXs-puro vector[39] with a N-terminally V5 and C-terminally FLAG. Human Xkr4 (hXkr4), mXkr8, hXkr8, mXkr9, and hXkr9 were constructed into plenti-IRES-puro vector[39] tagged with a N-

terminally V5 and C-terminally FLAG. mXkr4ΔC was cloned into plenti vector tagged with SPOT at N-terminal and a FLAG tag at C-terminal[39]. In case of the continuously activated mutant mXkr4ΔC Q332E (aXkr4) and other mutants, aXkr4 D123N, aXkr4 D127N, aXkr4 E310Q, aXkr4 D123A, aXkr4 D127A, aXkr4 E310A, aXkr4 D123C, aXkr4 V124C, aXkr4 G125C, aXkr4 T126C, aXkr4 D127C, aXkr4 E310C, aXkr4 D123C/E310C, aXkr4 V124C/E310C, aXkr4 G125C/E310C, aXkr4 T126C/E310C, aXkr4 D127C/E310C, aXkr4 D123K, aXkr4 D123R, aXkr4 G125K, aXkr4 G125R, aXkr4 D127K, aXkr4 D127R, aXkr4 E310K, aXkr4 E310R were constructed into the pMXs vector tagged V5 tag at N-terminus, a FLAG tag and tagRFP at the C-terminus. To transiently express mXkr4ΔC in HEK293 cells, mXkr4ΔC tagged with a N-terminally V5, and C-terminally HRV3C cleavage sites, FLAG tag and monomeric EGRP (mEGFP), was constructed into pNEF vector[15]. To express Xkr4 in Baculovirus mediated expression, human Xkr4ΔC was constructed into pEG Bacmam verctor with V5 at the N-terminus, and a FLAG tag, HRV3C cleavage site, mEGFP tag, His10 tag at the C-terminus. Human XRCC4 (hXRCC4) was constructed as previous description[39]. hXRCC4 and its mutants: hXRCC4 I266G, hXRCC4 K270A, were constructed into plenti vector, and tagged with tagRFP at the C-terminus.

For expression of MFG-E8, MFG-E8 D89E[54] mutants was used in this study, which was cloned into plenti vector with a 3×GGGS linker, mEGFP tag and His_8 tag at the C-terminus.

To express human cDNA of XRCC4 (hXRCC4) using bacteria, the full-length human cDNA of hXRCC4 was applied to codon optimization, followed by synthesis at Sangon Biotech. The synthesized hXRCC4 was cloned into the pCold1 vector with His8 tag at the C-terminus. The C-terminal fragment (XRCC4/C, 265-366), the point mutants (XRCC4/C I266G, XRCC4/C R270A) were cloned into pGEX-5X1 vector with His8 tag at the C-terminus, and an enterokinase (EK) cleavage sites (Asp-Asp-Asp-Asp-Lys) was introduced into the N-terminus of XRCC4/C, XRCC4/C I266G, and XRCC4/C R270A to expose the I266.

The bovine EK catalytic subunit (cEK) was applied to codon optimization, synthesized in Sangon Biotech, cloned into pGEX-5X1 vector with a EK cleavage sites at the N-terminus for self-activation.

2.4 Generation of cell lines

Ba/F3 cells deficient in TMEM16F and Xkr8, called BDKO cells, were established as previously described[39]. Retroviruses and Lentiviruses for transfection were generated as previously reported[39]. In

brief, Retroviruses components-expressing vectors, pGag-pol IRES bsr and pCMV-VSVG (RIKEN) and the target proteins expression vector pMXs or pMXs-puro were mixed at a ratio of 1:1:2, following by a mix with polyethylenimine MAX (PEI) (Polysciences) at a ratio of 1:3 in 150 mM NaCl solution, and added into HEK293T cells. Twenty-four h after transfection, five ml fresh medium was added into cells, and cells were cultured for 24 h more at 37 ℃. The supernatant of medium containing retroviruses was collected with 0.22 μm filter, and retroviruses was concentrated by centrifugation at 6,000 × for 16 h. Then, 500 ul fresh medium was mixed with 10 ul/ml polybrene, used to resuspend the virus, and added to 5×10^5 BDKO cells. Lentiviruses generation was performed with the pCMV-VSVG-RSV-Rev (RIKEN), pCAG-HIVgp (RIKEN) vector, and lentiviral vector, which virus was produced from HEK293T mediated by PEI. Five ml fresh medium was added into cells after 24 h transfection, and cells were cultured for another 24 h. The lentiviruses in supernatant were collected and filtered with 0.22 μm filter. To concentrate the virus, the supernatant was centrifuged at 6,000 × for 16 h. lentiviruses was resuspended with 0.5 ml fresh medium containing 10 μg/ml polybrene and used to infect the PLB (gifted from Prof.W.Hiraoka).

2.5 Expression and purification of Xkr4

To express human Xkr4ΔC (hXkr4ΔC), the recombinant baculovirus P1 expressing hXkr4ΔC was used to infect the FreeStyle 293F cells at 2×10^6 cells/ml. Cells were cultured in FreeStyle 293 medium (Gibco) containing 2% FBS at 120 rpm, 37 ℃, 8% CO_2 for 24 h, and a final concentration of 10 mM sodium butyrate was added into the medium to improve the expression. After culturing for 12 h with sodium butyrate, the temperature was decreased to 30 ℃ for another 36 h culture, and cells were collected by centrifugation (6000 ×g, 4 ℃, 5 min).

For purification of hXkr4ΔC, cells were homogenized using a Dounce homogenizer in a hypotonic buffer (10 mM HEPES (pH 7.5), 10 mM $MgCl_2$, 20 mM KCl, 0.5 M Sucrose, 1 mM EGTA, 1 mM p-APMSF, protease inhibitor cocktail (nacalai tesque), and 1 mM NaF). The crude membrane was collected by centrifugation (100000 ×g, 4 ℃, 30 min). The crude membrane was homogenized twice in high osmolarity buffer (10 mM HEPES (pH 7.5), 10 mM $MgCl_2$, 20 mM KCl, 1 mM NaCl, 0.5 M Sucrose, 1 mM EGTA, 1 mM p-APMSF, protease inhibitor cocktail, and 1 mM NaF). To extract the membrane proteins, the membrane extraction was solubilized with solubilization buffer (10 mM HEPES (pH 7.5),150 mM NaCl, 1 mM $CaCl_2$, 1 mM p-APMSF, protease inhibitor cocktail, and 1 mM NaF) containing 0.9% LMNG (Antrace) and 0.1% GDN (Antrace) for 2 h. The supernatant was

collected by centrifugation (20000 ×g, 4 ℃, 20 min) and purified by Ni-NTA Agarose HP (Wako). Further purification was carried out by a size exclusion chromatography (SEC) column (Superdex Increase 200 10/300 GL, GE Healthcare), which was equilibrated with a column buffer (10 mM HEPES-NaOH (pH 7.5), 150 mM NaCl, 0.01% LMNG/GDN at a ratio of 1:1, 10% glycerol, 1 mM $CaCl_2$). SEC analysis was performed at 0.35 ml/min, and fractions containing hXkr4ΔC or dimer were collected at 39 to 40 min. All purification steps were carried out under 4 ℃. Pooled samples were concentrated using 100 kDa Amincon Ultra centrifugal filter (Merck) and flash frozen using liquid nitrogen, finally stored at -80 ℃ until use.

2.6 Expression of active catalytic enterokinase

Recombinant cEK protein was produced from *E.coli*. In brief, the cEK was constructed into pET-22b and introduced into *E.coli* BL21(DE3). To express the cEK, *E.coli* was cultivated at 37 ℃ in LB medium until the OD600 up to 0.6 to 0.8. A final concentration of 0.5 mM IPTG was added into the medium, and *E.coli* was further incubated at 37 ℃ for 4 h to express the cEK. After that, the *E.coli* pellet was collected using centrifugation at 6,000 ×g for 5 min, resuspended in lysis buffer (25 mM Tris-HCl (pH 7.5), 0.5 mM EDTA), lysed using sonication. To harvest the cEK inclusion bodies, the lysate was separated by centrifugation at 15,000 ×g, 4 ℃, 20 min, and the pellet was collected. Pellet was firstly washed at room temperature (RT) for 1 h using a solution containing 0.9% Triton X-100, and collected pellet by centrifugation at 15,000 ×g, 4 ℃, 20 min. The collected pellet was washed with 0.5% NaCl buffer at RT for 1 h for twice, further was dissolved using the denaturation buffer (50 mM Tris-HCl (pH 9.0), 10 mM EDTA, 8 M urea) at RT for 1 h. Added a final concentration of 10 mM β-mercaptoethanol into the denature solution and incubated at RT for 1 h, and finally the denatured sample was diluted into a renaturation buffer containing 50 mM Tris-HCl (pH9.0), 3 mM glutathione (GSH), and 1 mM glutathione disulfide (GSSG). The activated cEK was collected after 2 days incubation at 25 ℃ and stored at 4 ℃ until use.

2.7 Expression and purification of XRCC4

Full-length XRCC4 (WT), the C-terminus fragment XRRC4/C, and point mutants XRCC4/C I266G and XRCC4/C R270A were expressed using BL21(DE3). To induce the expression of proteins, BL21(DE3) was cultivated at 37 ℃ in LB medium, 0.5 mM IPTG was added into the medium when

the OD600 of BL21(DE3) was up to 0.6 to 0.8, and further incubated for overnight at 16 ℃ for XRCC4/C and its point mutants, at 15 ℃ for the WT. Collection of bacteria was performed at 6000 ×g, 4℃, 5 min. Collected pellet was resuspended with lysis buffer containing PBS and 10 mM imidazole and lysed by sonication. The supernatant was collected by centrifugation at 20,000 ×g, 4 ℃, 20 min. To purify the WT, the supernatant was loaded into the Ni-NTA Agarose HP (FUJIFILM) for the first purification, and further purification was done using a HiLoad 16/600 Superose 75 pg (AKTA purifier FPLC system, cytiva). In the case of XRCC4/C and its point mutants, the supernatant from the lyse was applied to the glutathione Sepharose (GE healthcare) and eluted in buffer containing 50 mM Tris-HCl (pH 8.0), 10 mM GSH. To remove the GST tag from XRCC4/C and mutants, the purified sample was diluted in the cleavage buffer containing 20 mM Tris-HCl (pH 8.0), 200 mM NaCl, 2 mM $CaCl_2$, and treated with cEK at a molar ratio of 1:8 (XRCC4/C: cEK) at 4 ℃ for overnight. The mixture of cleavage sample was enriched using the Ni-NTA Agarose HP (FUJIFILM), and eluted in the buffer containing 10 mM HEPES (pH 8.0), 150 mM NaCl, 200 mM imidazole. Further purification was performed by SEC with HiLoad 16/600 Superose 75 pg column (AKTA purifier FPLC system, cytiva), which was eluted with PBS. All purification was performed under 4 ℃. Purified samples of WT, XRCC4/C and mutants were concentrated using the 3 kDa cut-off Amincon Ultra centrifugal filter (Merck) and stored at -80 ℃.

2.8 Expression and purification of MFG-E8

MFG-E8 can detect PS exposure in the absence of extracellular Ca^{2+}. To produce the MFG-E8 proteins, CHO cells were selected to express the mutant MFG-E8 D89E which was tagged with 3×GGGS linker, monomeric EGFP, 3×GGGS linker, and 8×Histidine. CHO cells expressing MFG-E8 D89E were established with the lentiviral system, and the high expression of the MFG-E8 cell population (the top 0.5% of GFP-positive cells) was sorted using flow cytometry (FACS AriaII). The sorted cells were cultivated in 300 ml of MEM/Ham's F-12 (Wako) supplemented with 10% FBS and antibiotics for one day until the cells were up to 80% confluent, replaced the medium with fresh medium, but did not contain FBS. Then, the cells were incubated at 37 ℃, 5% CO_2 for another 4 days, and collected the medium from each two days. 0.1% TritonX-100 and 5% glycerol were added into the collected medium to stabilize the protein, and then were loaded into the Ni-NTA Agarose HP (FUJIFILM) for first purification with the elution buffer containing 300 mM imidazole, 25 mM Tris (pH 8.0), 150 mM NaCl. The collected MFG-E8 was concentrated using 50 kDa cut-off Amincon Ultra centrifugal filter

(Merck), and changed the buffer into HBSS buffer by dialysis. Finally, purified MFG-E8 was mixed with 0.1% BSA and stored at -30℃ until use.

2.9 Preparation of whole cell lysate

mXkr4ΔC in pNEF in plenti vector were transiently expressed in HEK293T cell mediated by PEI (3:1 of PEI and plasmid). One day later after transfection, cells were collected using scraper, washed with a cold PBS for twice, flash frozen the cells pellet with liquid nitrogen, and stored at -80 ℃ until use. Cell pellet was thawed on ice and resuspended in solubilization buffer containing 10 mM HEPES-NaOH (pH 7.5), 100 mM 6-aminocaproic acid, 140 mM NaCl, 1% detergent, 10% glycerol, 1 mM indicated metal ions or 0.5 mM EGTA, 1 mM p-APMSF, protease inhibitor cocktail set V (EDTA free) (FUJIFILM), 1 mM NaF, and incubated on ice for 1h. The supernatant was collected using centrifugation at 20,000 ×g, 4 ℃, 20 min. The protein concentration was quantified by the BCA Protein Assay kit (Thermo Fisher Scientific).

2.10 Collection of dimer fraction Xkr4

pNEF vector encoding mXkr4ΔC or aXkr4, tagged mEGFP, was transiently expressed in HEK293T cells. The whole cell lyase was prepared as section 2.9. To purify the dimer, the whole cell lysate was applied into SEC with Superdex Increase 200 10/300 GL (GE Healthcare) with column buffer containing 10 mM HEPES-NaOH (pH 7.5), 150 mM NaCl, 0.01% LMNG/GDN (1:1), 10% glycerol, 1 mM $CaCl_2$ or 0.5 mM EGTA. The dimer peak was collected, based on the GFP signal, flash frozen in liquid nitrogen, and stored at -80 ℃ until use.

2.11 Thermostability assay of Xkr4

The collected mouse Xkr4ΔC or aXkr4 dimer were diluted with column buffer (section 3.12) into a relative fluorescence unit (RFU) of 2000 which were measured by the fluorescent microplate reader, then, the diluted dimer was incubated at different temperatures (4, 16, 25, 37 ℃) for 1 h. The aggregation was removed by centrifugation (20,000 ×g, 4 ℃, 20 min) and the supernatant was collected. The supernatant was diluted again into the fluorescence intensity at 800 RFU to perform

Blue Native (BN)-PAGE. Quantification of the protein level was performed using ImageJ (https://imagej-nih-gov.kyoto-u.idm.oclc.org/ij/), in which the total amount of proteins including dimer and monomer before incubation was defined as 100%.

2.12 Blue Native-PAGE

BN-PAGE was performed as previously descripted[39]. In brief, samples were adjusted to an appropriated concentration with a low detergent concentration and loaded into NativePAGE Novex 4%-16% (wt/vol) Bis-Tris gels (Thermo Fisher Scientific). The 1st electrophoresis was performed for 30 min at 150 V in 0.02% CBB G-250 Cathode buffer, and 2nd electrophoresis was performed for 2 h at 150 V in a lower concentration of 0.002% CBB G-250 in Cathode buffer. The NativePAGE was soaked into the SDS buffer containing 20 mM Tris-HCl (pH 8.3), 190 mM Glycine, 0.1% SDS at RT for 20 min to denature the proteins. The proteins were transferred from gel to a PDVF membrane (Sigma) at 0.1 A for 1 h. The PDVF membrane was blocked using 5% skim milk in TBS-T buffer containing 25 mM Tris-HCl (pH 7.5), 150 mM NaCl, 0.05% Tween 20 (Bio-Rad) at RT for 3 h. The skim milk was replaced with fresh one for each 1 h. Mouse Xkr4ΔC or aXkr4 or human Xkr4ΔC were detected with anti-V5-HRP antibody (Thermo Fisher Scientific) in 6,000 dilutions.

2.13 Western blot

The whole cell lysate was diluted with 5 × sample loading buffer (200 mM Tris-HCl (pH 6.8), 10% SDS, 25% glycerol, 5% β-mercaptoethanol, 0.5% bromophenol blue), and incubated at RT for overnight for Xkr4 denaturation. Samples were applied to the polyacrylamide gel (BIOCRAFT), and performed electrophoresis at 35 mA for 40 min. PDVF membrane transformation was performed at 0.1 A for 1 h, and blocked at RT for 30 min with 5 % skim milk in TBS-T buffer. Proteins was detected with anti-V5-HRP antibody (Thermo Fisher Scientific) in 6,000 dilutions, and anti-tagRFP rabbit pAb (Evrogen) in 4,000 dilutions which follow was detected using ploYclonal goat anti-rabbit immunoglobulins/HRP (DAKO) at 10,000 dilutions.

2.14 Immunoprecipitation

To perform immunoprecipitation, XRCC4 fused with tagRFP and Xkr4ΔC tagged with a N-terminal SPOT tag and a C-terminal FLAG were expressed in PLB cells of XRCC4 knockout[39]. The cells were collected and replaced with a fresh RPMI medium in one day before apoptosis stimulation. The cells were seeded in a pre-warmed fresh RPMI medium and cultivated at 37 ℃ for 1 h. Apoptosis was induced by adding a final concentration of 10 μM STS. After that, the membrane fractions were prepared from the apoptotic cells as described above, and solubilized in solubilization buffer containing 1% DDM/CHS. The solubilized samples were mixed with the anti-SPOT nanobody-coupled magnetic agarose beads (SPOT-Trap, Chromo Tek) at 4 ℃ for 2 h. Then the beads were washed using the cold wash buffer containing 20 mM Tris-HCl (pH 7.5), 100 mM 6-aminocaproic acid, 50 mM NaCl, 1 mM $CaCl_2$, and 0.03% DDM/ 0.003% CHS for triple. The beads were applied to mass spectrometry assay or eluted using the buffer containing 5 × sample loading buffer as described above and analyzed by western blot.

2.15 Mass spectrometry for protein-protein interaction

Mass spectrometry was performed as in the previous report[39]. The magnetic agarose beads which were prepared from immunoprecipitation were further washed using the 5 × sample loading buffer for 2 times, and incubated with 200 ng trypsin/Lys-C mix (Promega) at 37 ℃ for 16 h to digest the protein on the beads. GL-Tip SDB (GL Sciences) was used to reduce alkylate, acidify, and desalted the digested proteins. The samples were evaporated in the SpeedVac concentrator, and resuspended with 0.1% trifluoroacetic acid and 3% acetonitrile (ACN). LC-MS/MS analysis was performed using the EASY-nLC 1200 UHPLC which was connected with an Orbitrap Fusion mass spectrometer through a nanoelectrospray ion source (Thermo Fisher Scientific). A 75 μm inner diameter × 150 mm C18 reversed-phase column (Nikkyo Technos) was used to separate the peptides using a linear 4%–32% ACN gradient for 0–100 min, and followed with a high percentage at 80% ACN for 10 min. The mass spectrometer was performed in a data-dependent acquisition mode which a maximum duty cycle at 3 s, and the MS1 spectra were measured basing on a resolution of 120,000, an automatic gain control (AGC) target of 4×10^5 and a mass range from 375 to 1,500 m/z. HCD MS/MS spectra were got in the linear ion trap of an AGC target of 1×10^4, an isolation window of 1.6 m/z, a maximum injection time of 100 msec and a normalized collision energy of 30, and dynamic exclusion was set to 20 s. Based on the SwissProt database, the raw data was analyzed against the restricted to H. sapiens and

mouse Xkr4 protein by Proteome Discoverer version 2.3 (Thermo Fisher Scientific) with Sequest HT search engine, and The parameters for searching were employed as described: (a) trypsin as an enzyme with up to two missed cleavages; (b) precursor mass tolerance at 10 ppm; (c) fragment mass tolerance of 0.6 Da; (d) carbamidomethylation of cysteine as a fixed modification; and (e) acetylation of protein N terminus and oxidation of methionine as variable modifications. Peptides were filtered according to the false-discovery rate of 1% with the percolator node. The precursor ions quantifier node was used for Label-free precursor ion quantification, and normalization was carried out with the total sum of abundance values for each sample over all peptides.

The selected peptides of mouse Xkr4 and human XRCC4 were measured by PRM, which is an MS/MS-based targeted quantification method basing on the high-resolution MS. LC-MS/MS analysis was performed on an EASY-nLC 1200 UHPLC which was connected to a Q Exactive Plus mass spectrometer by a nanoelectrospray ion source (Thermo Fisher Scientific). Targeted MS/MS scans were acquired by a time-scheduled inclusion list at a resolution of 70,000, an AGC target of 2×10^5, an isolation window of 4.0 m/z, a maximum injection time of 2 s, and a normalized collision energy of 27. Time alignment and relative quantification of the transitions were performed using the PinPoint version 1.4 (Thermo Fisher Scientific).

2.16 Apoptotic stimulation with staurosporine

PLB cells expressing the target protein were collected and cultured in a fresh medium one day ago prior to the examination. On second day, PLB cells was collected and resuspend in pre-warmed fresh medium at a cell concentration at 1×10^6 cells/ml. The cells were cultivated at 37 ℃ for 1 h more, a final concentration of 10 μM STS was introduced into the medium. The cells were subsequently cultivated at 37 ℃ for 3 h.

2.17 Thapsigargin treatment

BDKO cells that expressed aXkr4 were washed and resuspended using the pre-warmed fresh medium. Subsequently, cells were cultivated at 37 ℃, 5% CO_2 incubator for 1 h. A final concentration of 4 μM Fluo4-AM (Dojindo) was added into cells, and cells were incubated for 30 min. Afterward, the thapsigargin (Wako) was introduced into the medium at a final concentration of 1 μM. To estimate the

intracellular Ca^{2+} level, the cells were harvested and washed with pre-chilled HBSS buffer, and then suspended in 200 μL of HBSS containing 0.5 mM EGTA or do not. The Fluo4-AM signal was analyzed by Flow cytometry. In the case of the PLS activity assay, the cells were treated with thapsigargin as above described, and analyzed the PLS using NBD-PC through the flow cytometry.

2.18 Apoptotic stimulation with ultraviolet-irradiation

Apoptotic stimulation was carried out following the procedure which was previously described[39]. In brief, PLB cells expressing target proteins were suspended in PBS and subsequently exposure on the UV-irradiation, cells expressing Xkr4 was performed at 2000 J/m^2 (CL-1000 (253 nm) crosslinker), while cells expressing Xkr8 or Xkr9 were irradiated at 200 J/m^2. The UV treated cells were harvested and cultivated in pre-warmed fresh medium at 37 ℃, 3 h for cells expressing Xkr4 and 2 h for cells expressing Xkr8 and Xkr9. Finally, the cells were applied to the PLS assay.

2.19 Electroporation of purified XRCC4

For the electroporation, 1×10^6 cells that expressing Xkr4ΔC or Xkr4FL were harvested, washed with opti-MEM (Gibco), and suspended in 100 μl opti-MEM. Then, a final concentration of 0.5 μM purified XRCC4 WT, XRCC4/C or its mutants was added and mixed with the cells. Electroporation was carried out using NEPA12 (Nepa Gene). After electroporation, the cells were collected and cultivated in 2 ml RPMI 1640 supplemented with 10% FBS at 37 ℃ for 1 h. Collected 5×10^5 cells and were used for the PLS analysis.

2.20 Introduction artificial disulfide bond

5×10^5 BDKO cells that expressed each Cys mutant were collected and washed with TBS buffer containing 25 mM Tris-HCl (pH 7.5), 140 mM NaCl. Subsequently, cells were treated with 1.1 mM copper-phenanthroline (CuP) (Tokyo Chemical Industry), which was dissolved in 20% ethanol, in TBS buffer at RT for 20 min or treated with 25 μM iodine solution (Wako) in TBS buffer at RT for 10 min. The treated cells were collected by centrifugation (400 ×g, 4 ℃, 2 min) and utilized for the PLS assay.

2.21 Phospholipid scrambling assay

PLS activity was examined with NBD-PC, NBD-sphingomyelin (NBD-SM) (Avanti Polar Lipids) and purified MFG-E8-GFP. 5×10^5 cells were harvested by centrifugation and washed with the cold HBSS buffer. Subsequently, the cells were suspended with 200 μl HBSS buffer containing a specific concentration of Ca^{2+} or 0.5 mM EGTA and incubated on ice for 10 min. Another 200 μl HBSS buffer mixing with a final concentration of 0.2 μM NBD-PC or 0.2 μM NBD-SM was added into cells. The cells were incubated on the ice for 12 min or 40 min for NBD-PC and NBD-SM, respectively. After that, the cells were treated with 400 μl HBSS buffer containing a final concentration of 5 mg/ml fatty acid-free BSA and 1 μg/ml DAPI to eliminate NBD-PC or NBD-SM on the cell surface on ice for more than 2 min. The PLS activity was measured using the flow cytometry. For A23187 (Sigma) treatment, the cells suspending with NBD-PC containing buffer were treated with a defined concentration of A23187 and incubated on ice for 4 min, the PLS activity was measured using flow cytometry.

For detection of exposed PS using purified MFG-E8-GFP, 5×10^5 cells were harvested by centrifugation and washed with cold HBSS buffer. Then the cells were suspended in 50 μl HBSS buffer which contained a specific concentration of Ca^{2+} and incubated on ice. After 10 min incubation, the purified MFG-E8-GFP was introduced into the cells. The cells were incubated on ice for 40 min, following by adding the HBSS buffer containing a final concentration of 1 μg/ml DAPI to separate the necrotic cells during the analysis. PS exposure was measured using flow cytometry. All of flow cytometry analysis were performed using a FACSLyric (BD Biosciences) or FACS ARIA2 (BD Biosciences).

2.22 Engulfment assay with dead cells

Engulfment assay was conducted as the method in previous report[39]. In brief, an 8-week-old female C57BL/6J mouse was injected with 2 ml of 3% thioglycolate into the peritoneum. The cells were harvested from the peritoneum of the mouse after 3 days, and suspended into DMEM supplemented with 10% FBS. For apoptosis induction, PLB cells that expressed SPOT-Xkr4-FLAG and XRCC4-tagRFP were induced the apoptosis using the UV, and were then labeled with pHrodo Green STP ester (Invitrogen) at a final concentration of 0.1 ug/ml. The apoptotic cells were co-incubated with thioglycolate-elicited peritoneal macrophages at 37 ℃ for 4 h. The macrophages were collected using trypsin/EGTA (Nacalai) at 37 ℃ for 3 min. A 400 dilution APC-labeled anti-CD11b antibody

(BioLgend) in CHES buffer containing 20 mM CHES pH 9.0, 150 mM NaCl, and 2% dialyzed FBS was added into the detached macrophages, which process was holding at 4 ℃ for 20 min. Finally, the macrophages were washed, suspended with the analysis buffer containing 20 mM CHES pH 9.0, 150 mM NaCl and supplemented with 0.25 μg/ml DAPI, followed analysis was performed using flow cytometry.

2.23 Measurement of membrane tension

Membrane tension experiments were performed as description in previous report[55]. In this study, BDKO cells expressing either the aXkr4 or aXkr4 E310A mutant were utilized and incubated at 4 ℃ for 45 min with 0.1 μg/ml anti-mouse basigin (Biolegend) in HEPES buffer (10 mM HEPES (pH 7.5), 140 mM NaCl, 1% BSA). After washing with HEPES buffer, the cells were incubated with 0.2 μg/ml anti-rat IgG biotin (Thermo Fisher Scientific) at 4 ℃ for another 45 min. The cells were washed and placed onto poly-L-lysine (0.05 mg/ml) pre-coated glass bottom dished (IWAKI), and bound with the streptavidin conjugated beads (SPHERO^{TM}). For the membrane tension analysis, the cells were cultivated with a specific DMEM medium, which does not supplement Ca^{2+}. The membrane tension was measured under RT with a different Ca^{2+} concentrations of 0 mM, 2 mM, or 5 mM Ca^{2+}.

The beads attaching on the cells were selected and pulled by the optical trap system (MMS-1064-200-2L/2E/2S, Sigma Koki) using a 1063 nm laser. A 100× oil objective (UPLSAPO100XO, NA = 1.4, Olympus) mounted on an inverted microscope (IX71, Olympus) was used for bead manipulation and cell visualization in bright field. Beads that adhered to the cell membrane were pulled away from the stationary laser trap using the motorize stage (BIOS-225T, Sigma Koki). During the process, a CCD camera (Zyla 5.5 cMOS, Andor) was used to capture the images for each 10 ms, and these images were utilized for the analysis of the membrane tension. Using the acquired images, force-extension curves were generated by computing the force F exerted on the trapped beads using the formula $F = K_x \Delta x$. Here, Δx represents the deviation of the trapped bead from its initial position, and the spring constant of the optical trap $K_x = 36.55$ [pN/μm]. To determine the membrane tension, a linear fitting approach was applied to the force-extension curves to obtain the membrane tension, which was analyzed by matplotlib 3.5.1 and numpy.

2.24 Prediction of Xkr4 structure

Xkr4 structure was predicted by RoseTTAFold[50] (https://robetta.bakerlab.org/submit.php), and the loop in mXkr4 was refined using Modeller 10.1. Software of the chimera 1.16 or chimeraX 1.4 was utilized for viewing the structure.

2.25 Molecular dynamic analysis

CafeMol[56] was used for all simulations, and protein analysis was performed by using the AICG2+ mode. In the coarse-grained model, the Cα atomic of each amino acid was represented as bead. Electrostatic and excluded volume interaction were utilized to model the interaction between beads. Time propagation was based on langevin dynamics, the temperature was fixed at 300 K, the dielectric constant was 78.0, and the monovalent ion concentration was 150 mM. The structure of aXkr4 was predicted using RoseTTAFold Server[50]. For stimulation of the "calcium bridge", a 'bridging effect' was applied to each pair of postulated primary calcium-binding residues including D123, D127, and E310, based on Hooke's law $E(r) = -k(r - r_0)^2$ (if $r < r_0$), in which k represents force constant, r represents the distance between the residues, and r_0 represents the equilibrium distance. To enforce the 'bridging effect', r_0 was setting to 5.0 Å and k to 5.0 $J/Å^2$.

3. Results

3.1 Xkr4 activation by XRCC4

Xkr4 forms a homodimer after cleavage of its C-terminus by caspases[13,39], but the dimer formation is not enough to activate Xkr4. To identify the activating factors, a "reviving screening" using sgRNA library was performed[39], in which sgRNA library was introduced into the *CAD* knockout PLB cells expressing a caspase-cleaved form of Xkr4 (Xkr4ΔC). As a result, the nuclear protein XRCC4, involving in DNA repair[57], was identified as the critical factor for activation of Xkr4[39]. To confirm that XRCC4 regulates Xkr4, *XRCC4* was knocked out in Xkr4ΔC-expressing PLB cells, and apoptosis were induced using staurosporine (STS). As shown in Fig. 5a, PLB cells lacking *XRCC4* completely lost the PLS activity, but the activity was rescued by expressing a XRCC4 wild type (WT), confirming that XRCC4 is necessary for activation of Xkr4 (Fig. 5a). However, exogenous expression of the C-terminal fragment of XRCC4 (XRCC4/C) failed to rescue the PLS activity, suggesting that exposure of the I266 without addition of Met is important for XRCC4/C to activate Xkr4, which is consistent with our previous report[39]. To examine this hypothesis, I expressed the XRCC4/C fragment as a GST-fusion protein in *E.coli* (Fig. 5b and c), purified using glutathione beads, and cleaved by enterokinase (rEK) to digest GST and expose I266 of the fragment. Then, purified proteins were introduced into Xkr4-expressing Ba/F3 cells, deficient in both *Xkr8* and *TMEM16F* (BDKO), using electroporation (Fig. 5d). As expected, the PLS activity was observed when the purified XRCC4/C was introduced into the Xkr4ΔC-, but not Xkr4 full length (FL)-, expressing BDKO cells (Fig. 5e). In contrast, XRCC4 WT and XRCC4/C mutants (I266G and R270A) failed to induce the PLS activity of Xkr4, strongly demonstrating that the C-terminal fragment of XRCC4 with I266 exposure regulated Xkr4 activation.

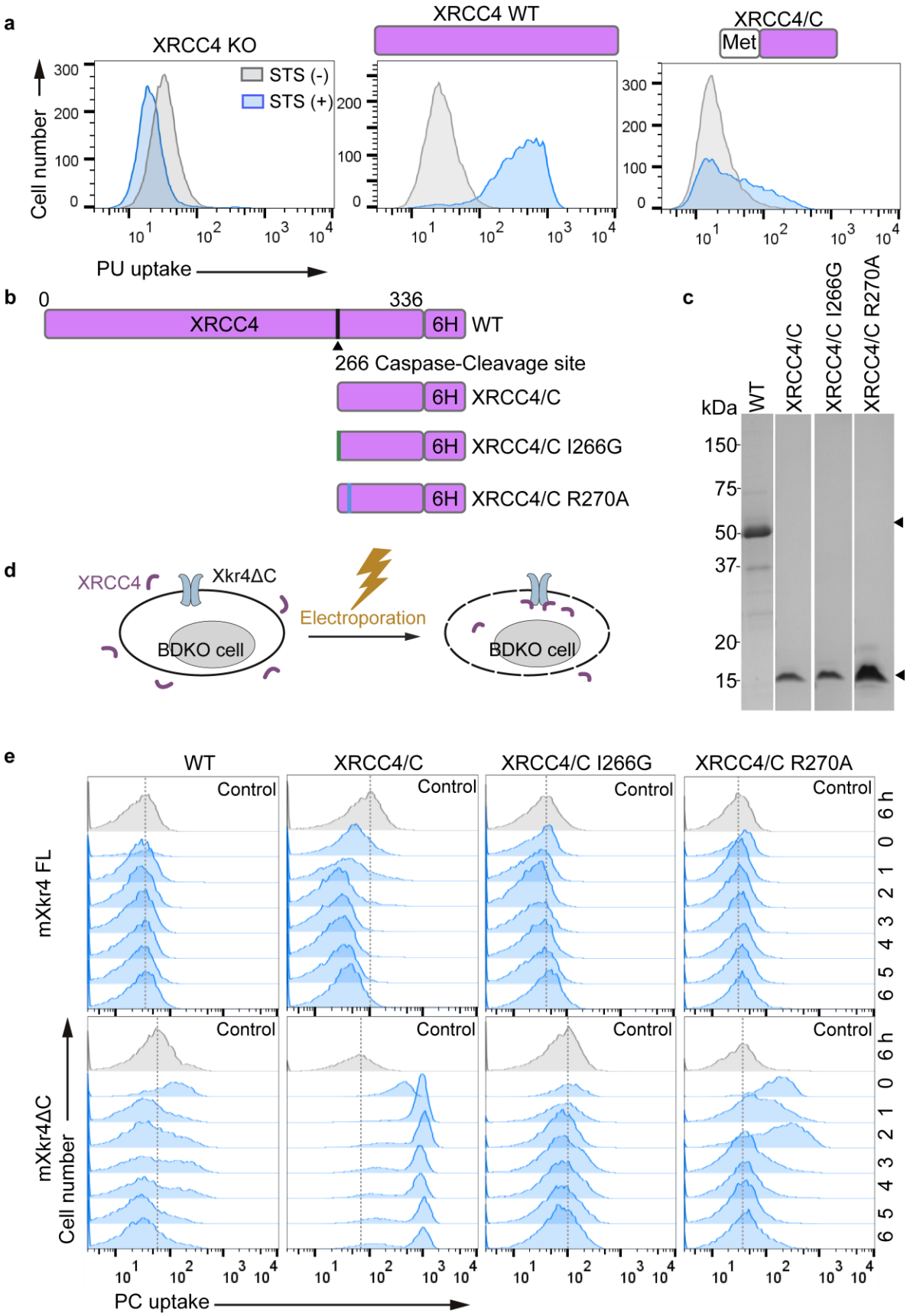
a
XRCC4 KO
XRCC4 WT
XRCC4/C
Met
STS (-)
STS (+)
Cell number
PU uptake
b
0
336
XRCC4
6H
WT
266 Caspase-Cleavage site
XRCC4/C
XRCC4/C I266G
XRCC4/C R270A
c
kDa
WT
XRCC4/C
XRCC4/C I266G
XRCC4/C R270A
150
75
50
37
20
15
d
XRCC4
Xkr4ΔC
BDKO cell
Electroporation
e
WT
XRCC4/C
XRCC4/C I266G
XRCC4/C R270A
Control
mXkr4 FL
mXkr4ΔC
Cell number
PC uptake
0 h
1
2
3
4
5
6

Fig. 5: Activation of Xkr4 by XRCC4 mutants a PLB cell were knocked out XRCC4 and expressed XRCC4 WT or the XRCC4/C (265-366) tagged tagRFP. The cells were induced apoptosis by STS and examined the PLS activity by NBD-PC using FACS. **b** Schematic representation of purified XRCC4 and its mutant variants, green and blue lines represent the mutation site in XRCC4/C R270A and XRCC4/C I266G, respectively. **c** SDS-PAGE of purified XRCC4 and its mutants. XRCC4 and its mutants were expressed and purified form E.coli. XRCC4/C, XRCC4/C R270A and I266G were cleaved by recombinant enterokinase after purification by Glutathione Sepharose to expose the the I266 or I266G, and final purified by size-exclusion chromatography. Purified proteins were examined by SDS-PAGE staining by CBB. **d** Schematic representation of electroporation to introduce XRCC4 and its mutants. **e** PLS activity assay with purified XRCC4 and its mutants. Using electroporation, purified XRCC4 or its mutants were introduced into Xkr4FL or Xkr4ΔC expressing BDKO cells. Control means electroporation without XRCC4.

3.2 A direct binding between Xkr4 and XRCC4

Next, I investigated how XRCC4/C regulates Xkr4 activation. I performed a protein-protein interaction screening using immunoprecipitation and mass spectrometry. PLB cells expressing both Xkr4ΔC fused with SPOT tag and XRCC4 were used to induce apoptosis with STS. To identify Xkr4 interactors, cell lysate prepared from SPOT-fused Xkr4ΔC-expressing cells was incubated with magnetic agarose beads coated by anti-SPOT nanobody (Fig. 6a). As shown in Fig. 6b, XRCC4 was precipitated with Xkr4 after apoptotic treatment when XRCC4 WT, but not XRCC4 R270A, was used, suggesting that XRCC4/C directly binds to Xkr4 to activate the PLS activity. The digested peptides from XRCC4 were quantified by mass spectrometry, and two peptides from the XRCC4 C-terminus showed a significant increase in the peptide amount in apoptotic cells compared to living cells. In apoptotic cells, the amount of two peptides was decreased when XRCC4 R270A was used, but not XRCC4 WT (Fig. 6c and d). These results also support that XRCC4/C directly binds to Xkr4 to activate it. To further confirm this finding, western blot was performed after immunoprecipitation. As shown in Fig. 6d, the cleaved fragment of XRCC4 was identified in XRCC4 WT-, but not in XRCC4 R270A-, expressing cells. Taken together, these results prove that XRCC4 regulates the PLS activity of Xkr4 through direct binding.

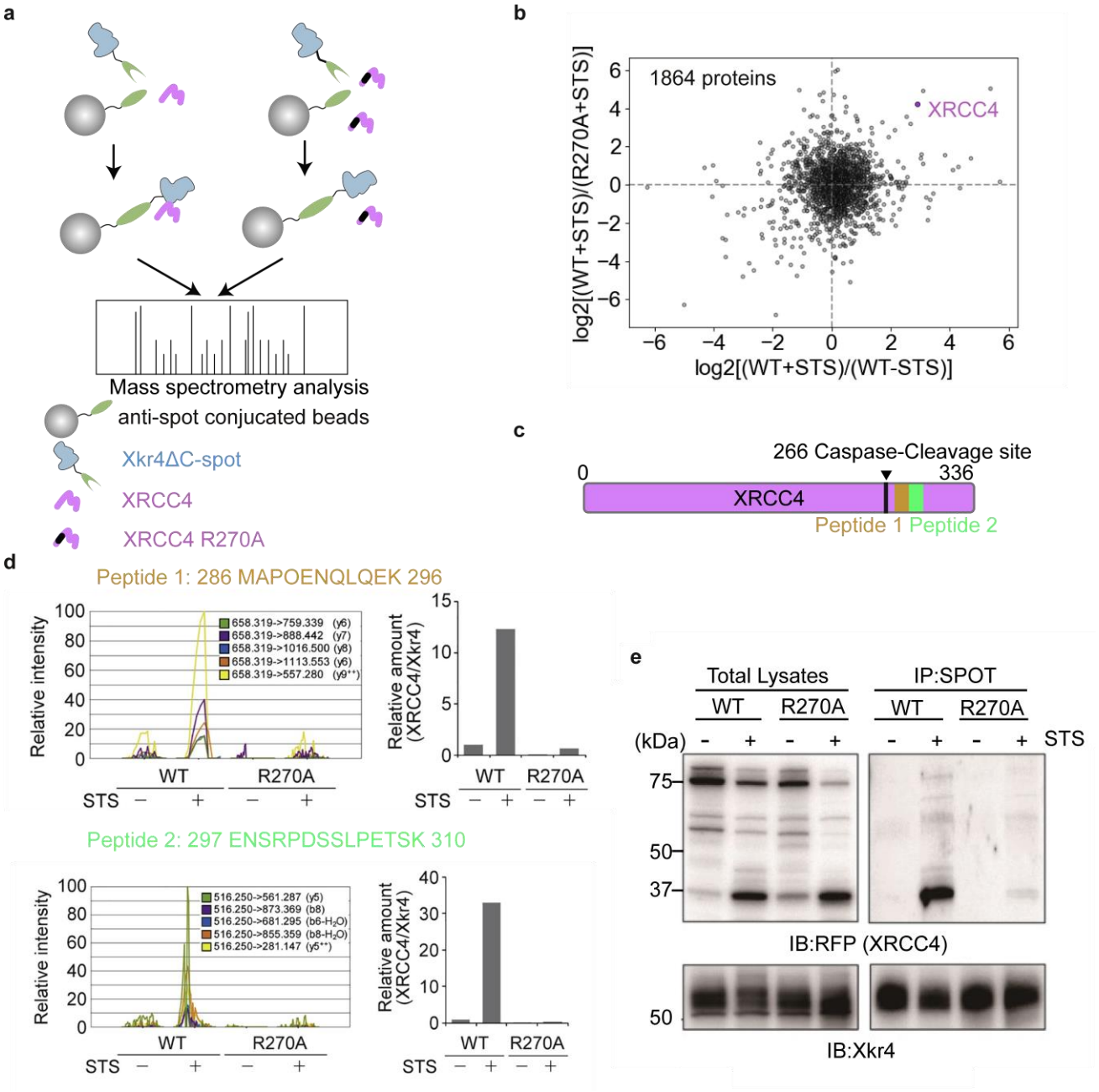

Fig. 6: A directing binding of Xkr4 and XRCC4 a Schematic representation of protein-protein interaction strategy through immunoprecipitation and mass spectrometry. **b** Mass spectrometry analysis. PLB cells expressing SPOT-Xkr4 ΔC-FLAG and XRCC4-RFP or the mutant R270A were induced apoptosis by STS. The membrane fragments were prepared from the apoptotic cells and solubilized in detergent. Solubilized samples were precipitated using the anti-SPOT magnetic agarose beads and applied to mass spectrometry to analyze the binding proteins of Xkr4ΔC. x axis: the fold changes of binding proteins in XRCC4 WT expressing cells between with STS and without STS treatment. y axis: the fold changes of binding proteins between XRCC4 WT and XRCC4 R270A expressing cells. **c** Schematic representation of XRCC4, which the caspase cleave site was highlighted with black line and arrow. The identified peptides from mass spectrometry were highlighted as yellow (peptide 1) and green (peptide 2) respectively. **d** Quantification of the XRCC4 peptides. The peptides were detected by targeted mass spectrometry (Left), and the relative amount of XRCC4 peptide bound with Xkr4 (right). **e** Immunoprecipitation of the XRCC4 WT and non-function mutant XRCC4 R270A. The whole cell lysate was prepared form PLB cells expressing SPOT-Xkr4 ΔC-FLAG and XRCC4-

RFP or the mutant R270A induced apoptosis by STS. The eluted samples were applied to western blot and detected by anti-RFP for XRCC4 or anti-FLAG for Xkr4.

3.3 Activation of the PLS activity of Xkr4 by Ca^{2+}

Through the protein-protein interaction screening, I found that Xkr4 was activated by dimer formation and a direct binding of the C-terminal fragment of XRCC4. It is noted that apoptotic PLB cells expressing Xkr4FL or Xkr4ΔC lost the PLS activity in term of PC uptake when the extracellular Ca^{2+} was removed, but was rescued when the extracellular Ca^{2+} was added (Fig. 7a), suggesting that Ca^{2+} is necessary to promote the PLS activity of Xkr4. The constitutively-active mutant Xkr4ΔC Q332E (aXkr4)[39], being activated without XRCC4/C, was expressed in BDKO cells to investigate the effects of Ca^{2+}. Similarly, aXkr4-expressing cells lost the PLS activity in the absence of extracellular Ca^{2+} but not in the presence of the extracellular Ca^{2+} (Fig. 7b), suggesting that Ca^{2+} is required for activation of Xkr4. The PLS activity can be defined not only by PC uptake, but also sphingomyelin (SM) uptake and phosphatidylserine (PS) exposure. Similar to PC uptake, SM uptake and PS exposure were disrupted when the extracellular Ca^{2+} was removed (Fig. 7c and d). In Fig. 5e, I showed that the introduction of purified XRCC4/C activates Xkr4 dimer to induce the PLS activity. To examine whether Ca^{2+} is necessary for XRCC4/C-mediated activation of Xkr4, I introduced the purified XRCC4, XRCC4/C or its mutants into the living BDKO cells expressing Xkr4FL or Xkr4ΔC. The PLS activity can be observed only when the XRCC4/C was introduced with in the presence of the extracellular Ca^{2+}, demonstrating that Ca^{2+} is necessary for activating Xkr4.

Exposed PS functions as an “eat signal” for engulfment by phogacytoes[7,8]. To understand the effects of the extracellular Ca^{2+} on engulfment, PLB cells expressing Xkr4 were used to induce apoptosis using ultraviolet (UV) and labeled with pHrodo, followed by incubation with mouse peritoneal macrophages in the presence of different concentrations of Ca^{2+}. Flow cytometry analysis showed that macrophages engulfed the apoptotic cells efficiently in an extracellular Ca^{2+} concentration-dependent manner (Fig. 7f), suggesting that the extracellular Ca^{2+} functions as a molecular switch for engulfment.

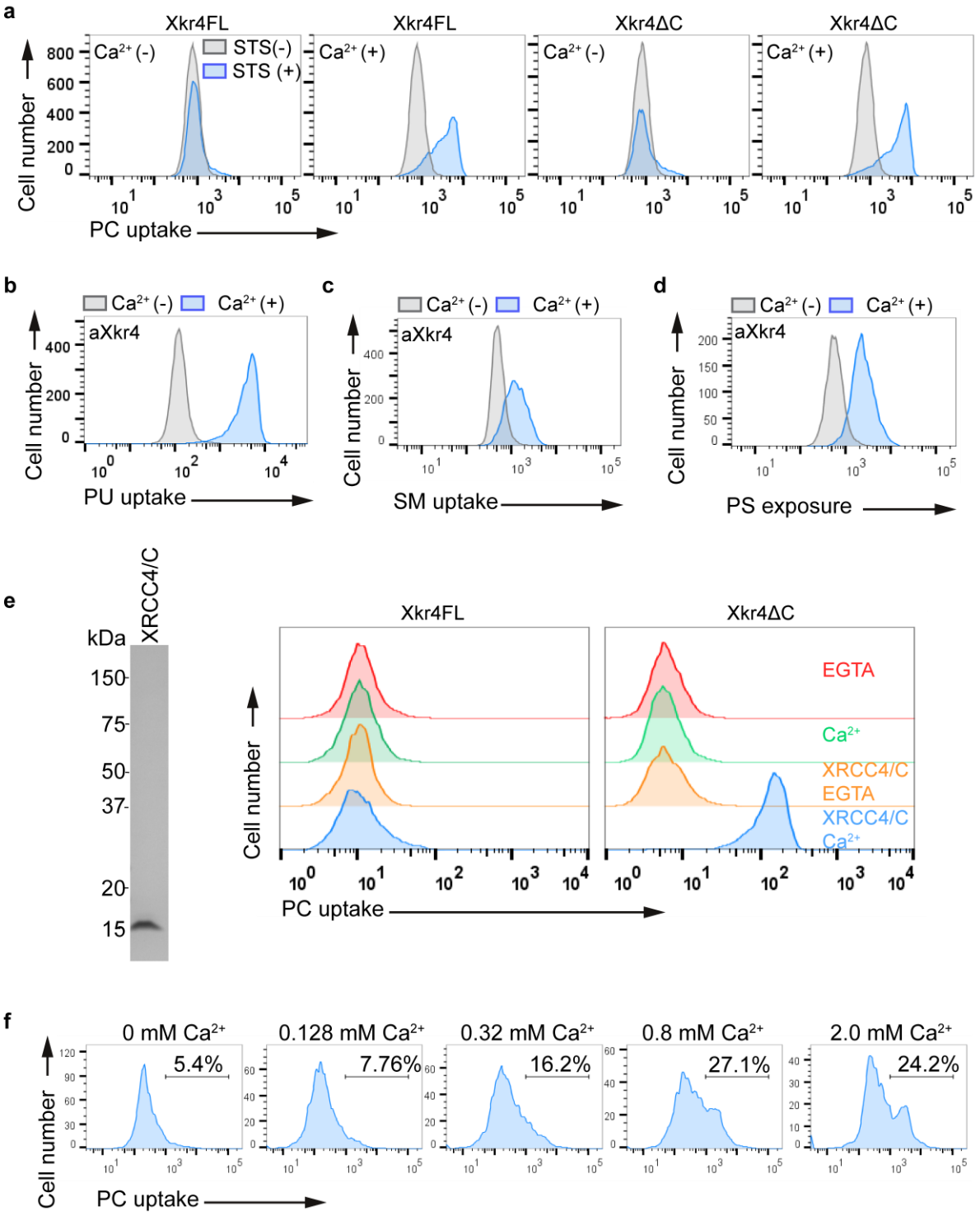

Fig. 7: Requirement of Ca^{2+} for mXkr4 activation a PC incorporation assay of the mouse Xkr4FL (mXkr4FL) or Xkr4ΔC (mXkr4ΔC) expressing PLB cells. PLB cells were introduced the apoptosis using 10 μM STS. The apoptotic cells were incubated with NBD-PC with or without Ca^{2+}, and the NBD-PC uptake was measured by FACS. **b-d** PLS activity assay of PC, Sphingomyelin (SM) and phosphotydeserine (PS) in aXkr4 expressing BDKO cells. The cells were incubated with NBD-PC, BND-SM or purified MFG-E8-GFP containing Ca^{2+} or not. The cells were incubated on ice with NBD-PC for 12 min (**b**), NBD-SM for 40 min (**c**), and MFG-E8 for 40 min (**d**). **e** PC incorporation assay of the mXkr4FL or Xkr4ΔC expressing PLB cells with purified XRCC4/C. Purified XRCC4/C was examined by SDS-PAGE with CBB staining (left). Cells was introduced the purified XRCC4/C

at final concentration of 0.5 μM by electroporation, and cultivated at 37 ℃ for 1 hr. PLS activity analysis was performed using NBD-PC with 1 mM Ca^{2+} or 0.5 mM EGTA, and measured by FACS (right). **f** Engulfment assay of apoptotic cells. PLB cells expressing mXkr4 were induced apoptosis using UV (2000 J/m^2) and following labeled by pHrodo. Engulfment was performed by incubated Labeled apoptotic cells with thioglycolate-elicited macrophages with a series of Ca^{2+} concentrations for 4 hr. The engulfment was measured using FACS by detecting the pHrodo signal.

3.4 Requirement of extracellular Ca^{2+} for Xkr4 activation

To further investigate the effects of Ca^{2+}, the PLS activity of aXkr4-expressing BDKO cells was analyzed in different concentrations of extracellular Ca^{2+}. As shown in Fig. 8a, PLS activity is increased in an extracellular Ca^{2+} concentration-dependent manner, suggesting that Ca^{2+} directly regulates Xkr4 activation. Treating aXkr4-expressing cells with the calcium ionophore A23187 increased the intracellular Ca^{2+}, but did not show a significant difference in PLS activity with or without A23187 (Fig. 8b), indicating that extracellular, rather than intracellular, Ca^{2+} is critical. Supporting this, thapsigargin treatment increased intracellular Ca^{2+} concentration (Fig. 8c), but failed to induce the PLS activity (Fig. 8d). These results suggest that the extracellular, but not intracellular, Ca^{2+} regulates Xkr4 activity.

Membrane tension is affected by changes in lipid distribution mediated by PLS[58]. To investigate whether the Ca^{2+} mediated-PLS activity regulates membrane tension, aXkr4-expressing cells were analyzed using an optical trap to measure the membrane tension changes in the presence or absence of extracellular Ca^{2+} (Fig. 8e). Cell membrane tension was significantly reduced in the presence of the Ca^{2+} compared to the absence of it (Fig. 8f and g), further confirming that the extracellular Ca^{2+} is necessary to activate Xkr4-mediated PLS.

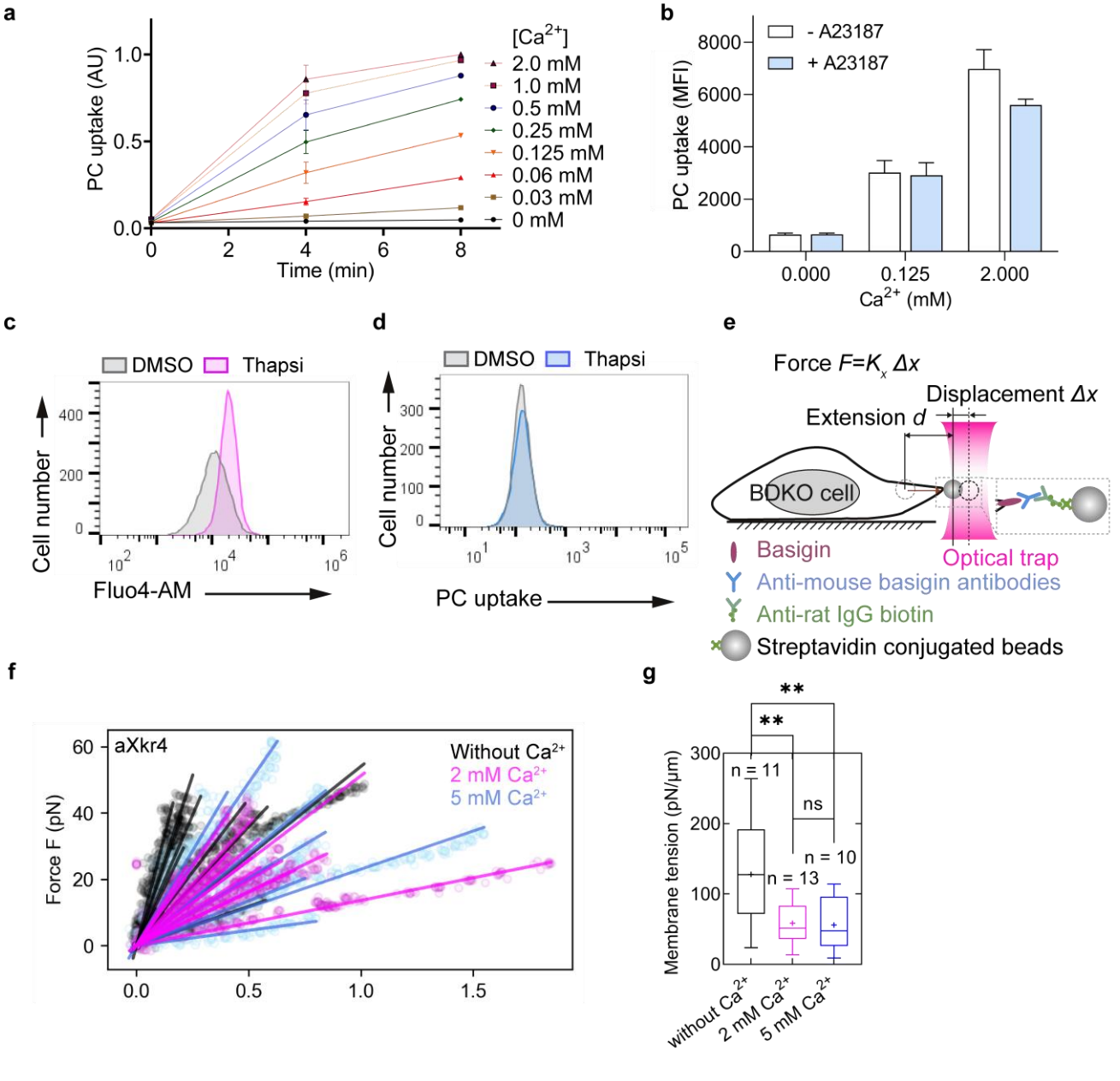

Fig. 8: Requirement of extracellular Ca^{2+} for Xkr4 activation. a a Ca^{2+} concentration dependent manner of Xkr4 PLS activity. aXkr4 expressing BDKO cells were treated with NBD-PC containing a series of different concentrations of Ca^{2+}, and the PLS activity was measured by FACS. Each condition was repeated for three times and shown with SD. AU represents arbitrary units. **b** A23187 treatment. aXkr4 expressing BDKO cells were treated a final concentration of 1 μM calcium ionophore A23187 and indicated Ca^{2+} concentration on ice for 4 min, and the PLS activity was measured by FACS. Each condition was repeated for four times and shown with SD. MFI represents the fluorescence intensity. **c** Inner Ca^{2+} measurement after Thapsigargin (Thapsi) treatment. aXkr4 expressing BDKO cells were incubated with a final concentration of 1 μM thapsi or DMSO in a same volume. Measurement of the inner Ca^{2+} was performed with a final concentration of 4 μM Fluo4-AM with or without 0.5 mM EGTA and analyzed by FACS. **d** Effect of Thapsi on PLS activity. aXkr4 expressing BDKO cells were incubated with a final concentration of 1 μM thapsi or DMSO in a same volume, then the PLS activity was performed through PC incorporation. **e** Schematic model for measurement of the membrane tension using optical trap. **f-g** Membrane tension of aXkr4. aXkr4 expressing BDKO cells was using

to measure the membrane tension with 2 mM (pink), 5 mM Ca^{2+} (blue) or without Ca^{2+} (black). The membrane tension was calculated from the linear fit of solid lines and shown as force-extension curve (**f**), Summary of the membrane tension was shown as box-plots (**g**). not significant. **, $p < 0.01$.

3.5 Activation of Xkr4 by metal ions

Ca^{2+}-binding proteins are often activated by other metal ions such as Sr^{2+}, Mg^{2+}, and Ba^{3+}due to their similar physical properties[59]. To investigate whether Xkr4 can be activated by other metal ions or not, the PLS activity of BDKO cells expressing aXkr4 were analyzed in the presence of 1 mM of different metal ions. Indeed, except for Ca^{2+}, several metal ions including Sr^{2+}, Mn^{2+}, and Tb^{3+} also induced the PLS activity (Fig. 9a). Among these, Sr^{2+} is the strongest to induce the PLS activity, but it has about a 7-folds decrease in affinity when compared to Ca^{2+}. In addition, Mn^{2+} and Tb^{3+} weakly activated Xkr4 with a drastic decrease in affinity (Fig. 9b and c) but Mg^{2+} and Ba^{2+} failed to activate Xkr4, suggesting an appropriate ionic radius (0.083 nm ~ 0.125 nm) is critical to activate Xkr4: Mg^{2+} (0.072 nm), Mn^{2+} (0.083 nm), Tb^{3+} (0.092 nm),Ca^{2+} (0.100 nm), Sr^{2+} (0.125 nm), Ba^{2+} (0.136 nm)[60–62]. Compared to Ca^{2+} in ionic radius, Mn^{2+} is smaller, but still activates the PLS activity, suggesting that the binding site in Xkr4 is flexible.

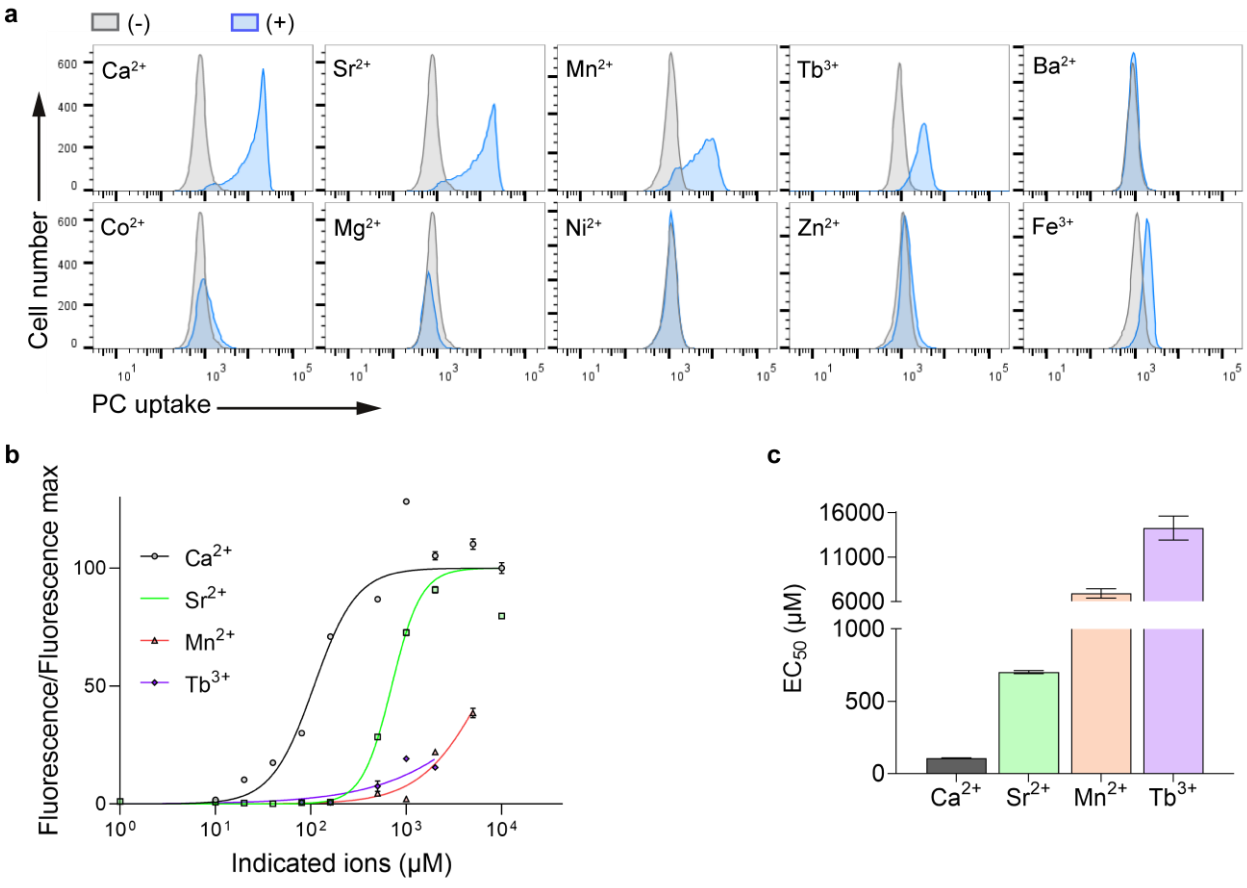

Fig. 9: Activation of Xkr4 with metal ions a PLS activity of aXkr4 was affected by metal ions. aXkr4 expressing BDKO cells were treated with a final concentration of 1 mM different metal ions including $CaCl_2$, $SrCl_2$, $MnCl_2$, $TbCl_3$, $BaCl_2$, $FeCl_3$, $CoCl_2$, $MgCl_2$, $NiCl_2$, or $ZnCl_2$, and the PLS activity was measured using NBD-PC by FACS analysis. bule represents that indicated metal ions were added, grey represents there are no metal ions. **b** the does-response curves of aXkr4. aXkr4 expressing BDKO cells were treated with a different concentration of $CaCl_2$, $SrCl_2$, $MnCl_2$, or $TbCl_3$, and the PLS activity was performed using NBD-PC by FACS analysis, and quantified PSL activity based on MFI. Each condition was performed tree times and shown as SD. The data of 10 mM Mn^{2+} and Tb^{3+} of 5 mM and 10 mM were not utilized for this analysis because the cells were died under those concentrations. **c** Half maximal effective concentration (EC50) of metal ions for PLS activity of Xkr4. According to the dose-response curve in (**b**), the EC50 was calculated for each metal ion, and shown as histogram. The Averages of triplicates were shown as SD.

3.6 Prediction of the potential Ca^{2+}-binding site

In Xkr family members, Xkr4, Xkr8, and Xkr9 function as a scramblase and induce the PLS activity after caspase-mediated cleavage of their C-terminal region[13]. To examine the activation of Ca^{2+} in Xkr family members, PLB cells expressing mouse and human Xkr4, Xkr8 or Xkr9 were used to induce apoptosis with UV and applied to the analysis of the PLS activity in the presence or absence of 1 mM Ca^{2+} or Sr^{2+}. As shown in Fig. 10a and b, all Xkr4, Xkr8 and Xkr9 were activated by the extracellular Ca^{2+} and Sr^{2+}. These findings suggest that Ca^{2+}-mediated PLS activity is conserved within Xkr family members in both human and mouse species.

To find out the potential Ca^{2+}-binding sites, I aligned the mouse and human Xkr4, Xkr8, and Xkr9, and searched for the conserved negatively-charged amino acids, potentially interacting with positively-charged Ca^{2+} (Fig. 10c). Because the extracellular Ca^{2+} is important to activate Xkr4 (Fig. 8b and d), I initially searched for the Ca^{2+}-binding sites in the extracellular region, but could not identify them. The another scramblase TMEM16 family are activated by the intracellular Ca^{2+}, and the Ca^{2+}-binding sites locate in the TM regions[28,63]. According to this knowledge, I hypothesized that the Ca^{2+}-binding site in the Xkr family located in the TM regions. Then, I highlighted negatively-charged amino acids in the TM regions to identify the candidate residues. By taking into account the 3D structures of Xkr8 and Xkr9[36,37], and the predicted structure of Xkr4, predicted by RoseTTAFold server[50], I finally identified the potential Ca^{2+}-binding site: D123 and D127 on TM1, and E310 on TM3 of Xkr4 form a Ca^{2+}-binding site that can be accessible from the extracellular region (Fig. 10c-h). The side chains of these three amino acids were oriented inward to the TM regions, implying that D123, D127 and E310 together form a Ca^{2+}-binding site.

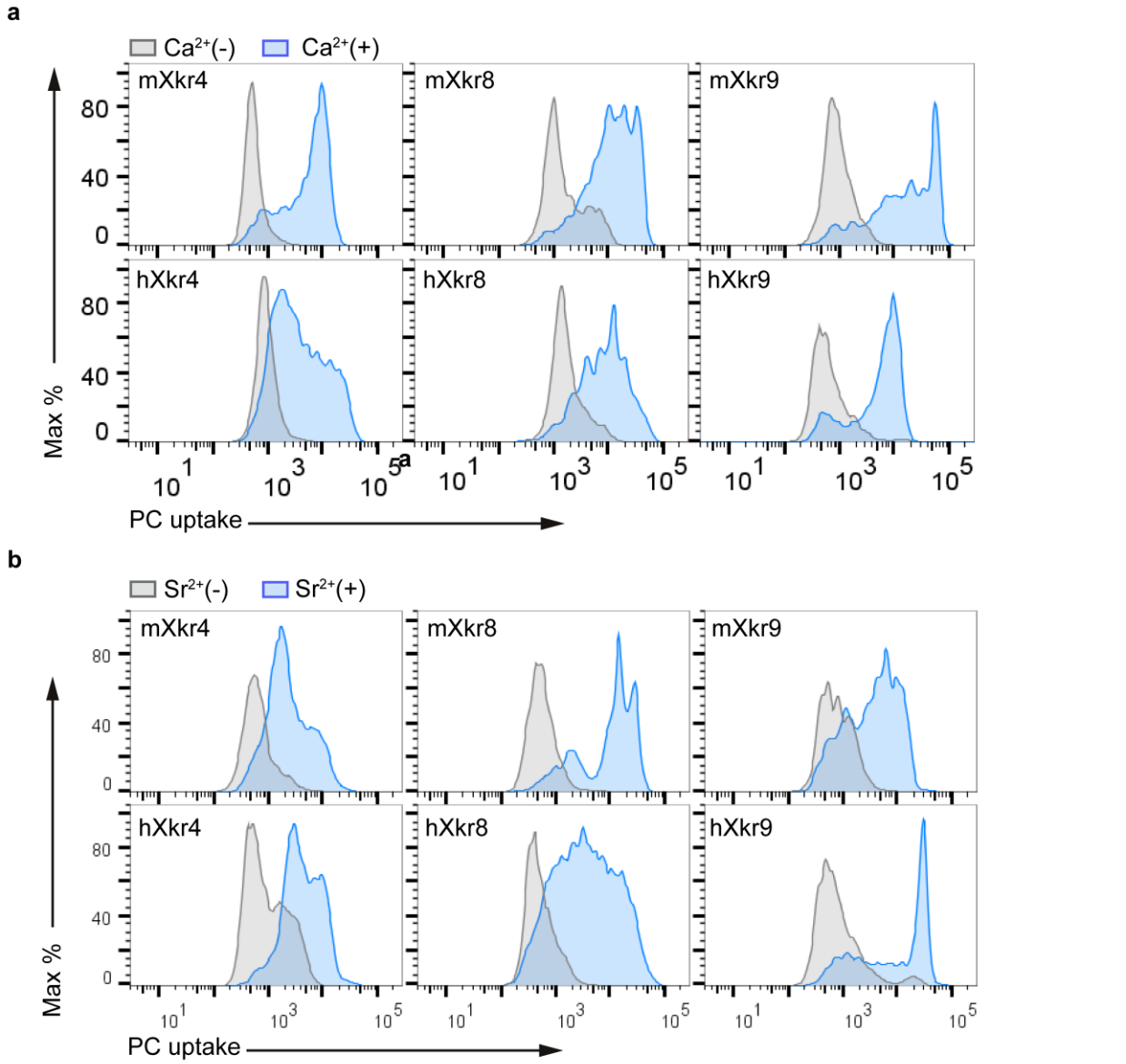
a
Ca2+(-)
Ca2+(+)
mXkr4
mXkr8
mXkr9
hXkr4
hXkr8
hXkr9
Max %
PC uptake
b
Sr2+(-)
Sr2+(+)
mXkr4
mXkr8
mXkr9
hXkr4
hXkr8
hXkr9
Max %
PC uptake

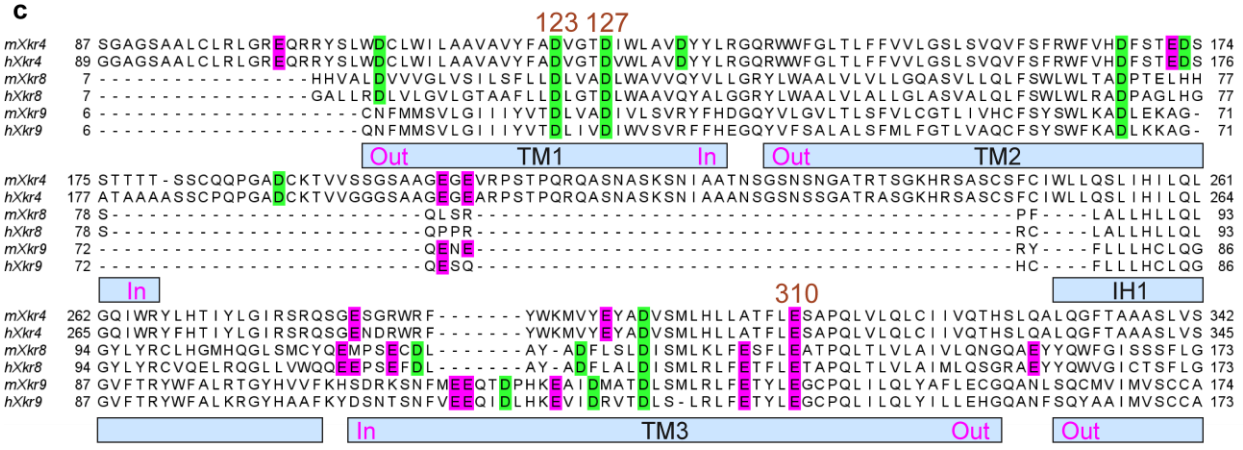
c
123 127
Out
TM1
In
Out
TM2
In
310
IH1
In
TM3
Out
Out

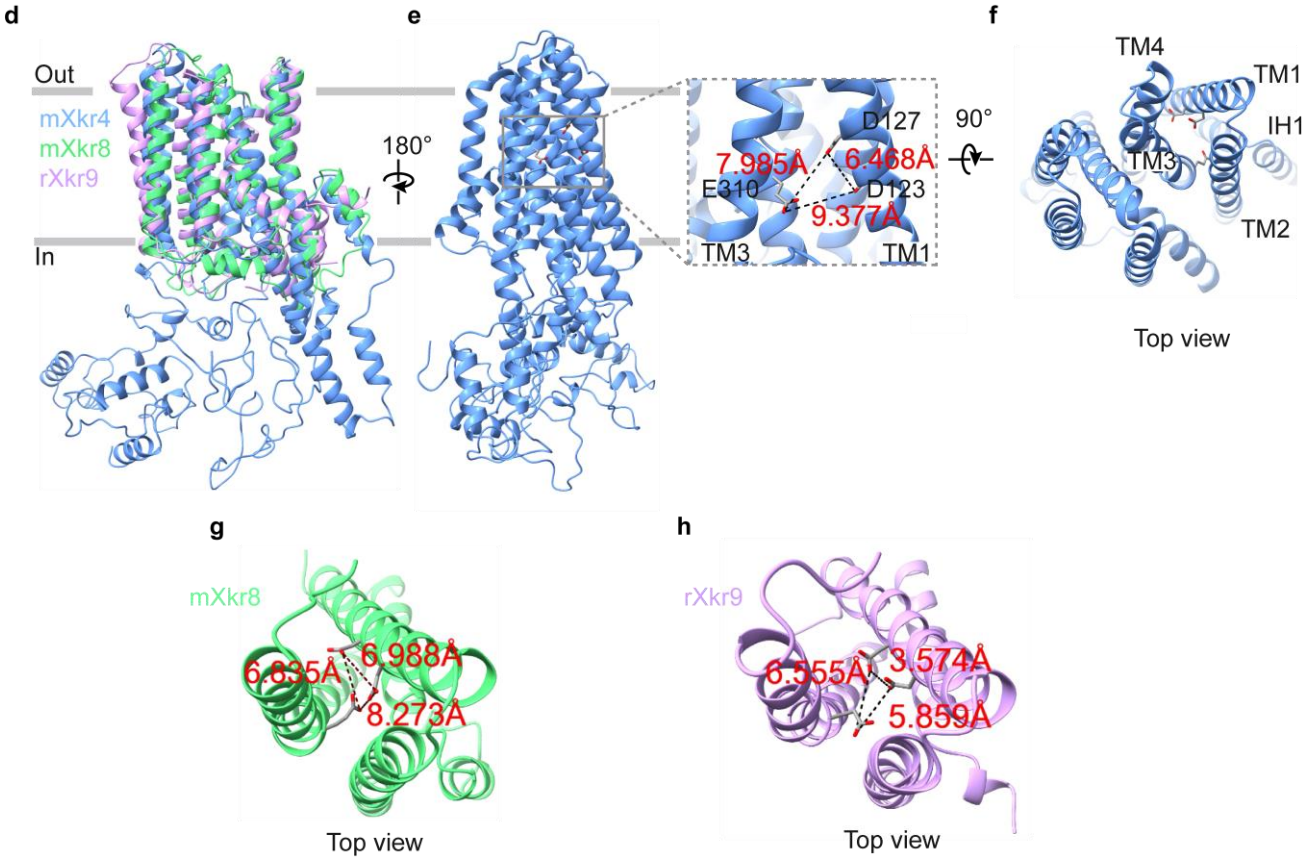

Fig. 10: Potential Ca^{2+}-binding sites a, b Effects of Ca^{2+} on PLS activity of mouse (m) or human (h) Xkr4, Xkr8, or Xkr9. PLB cells were induced apoptosis using UV: 2000 J/m^2 for Xkr4 expressing cells, 200 J/m^2 for Xkr8 and Xkr9 expressing cells, and cultivated at 37 °C for 3 h of Xkr4, and 2 h of Xkr8 and Xkr9. The PLS activity was measured by NBD-PC in the presence of a final concentration of 1 mM Ca^{2+} (**a**) or Sr^{2+} (**b**) or absent both metal ions. **c** Sequence alignment of mouse and human Xkr4, Xkr8, and Xkr9. The highly conserved Asp and Glu in Xkr4, Xkr8 and Xkr9 are highlighted in green and purple respectively, and potentially Ca^{2+}-binding residues according to the mXkr4 were marked using the red character numbers. **d-h** Structure analysis of potential Ca^{2+}-binding sites in predicted Xkr4, which was predicted by RoseTTAFold and refined by Modeller for the loop, mouse Xkr8 (spring green, PDB: 7DCE), and rat Xkr9 (violet, PDB:7P16). View of comparation of Xkr4, and Xkr8 and Xkr9 (**d**). The potential Ca^{2+}-binding sites was shown as sticks (oxygen: red) in Xkr4 with a side view (**e**) and top view (**f**), and these sites were shown in Xkr8 (**g**) and Xkr9 (**h**) with a top view. The distance of each residue was measured and shown as black dash lines.

3.7 Examination of the potential Ca^{2+}-binding site

After narrowing down the potential Ca^{2+}-binding site, I investigated the impact of the identified residues on the Xkr4 activity. Xkr4 was mutated in the potential Ca^{2+}-binding site and expressed in BDKO cells to observe their effects on the PLS activity. To prevent protein instability caused by the drastic changes in the side chain, D123, D127 and E310 were mutated into D123N, D127N, and E310Q, respectively. Among these mutants, D127N and E310Q showed a remarkable reduction in the PLS

activity (Fig. 11a and b) and in affinity to Ca^{2+}, suggesting that the negatively-charged oxygen in D127 and E310 directly interacts with Ca^{2+}. In contrast, the mutation D123N has a slight decrease in the PLS activity (Fig. 11a and b), implying that the non-charged oxygen of D123 plays a role in interacting with Ca^{2+}. To further examine the role of side chains, Ala mutants were generated: D123, D127 and E310 were mutated into D123A, D127A, and E310A, respectively. As expected, all mutants showed a drastic decrease in the PLS activity and in a low affinity to Ca^{2+} (Fig. 11a and c). These results demonstrated that D123, D127, and E310 associates with Ca^{2+}. When the PLS activity was analyzed using these mutants with Sr^{2+}, similar results were obtained (Fig. 11d and e), further supporting that D123, D127, and E310 coordinate Ca^{2+} binding. To investigate the impact of these three residues, I chose the E310A mutant for the analysis of membrane tension. Using the optical trap, I evaluated the membrane tension of cells expressing the aXkr4 E310A in the presence or absence of extracellular Ca^{2+}. As a result, membrane tension was not changed with or without Ca^{2+}, suggesting that D123, D127, and E310 interacts with Ca^{2+} to induce Xkr4-meidated PLS (Fig. 11f and g).

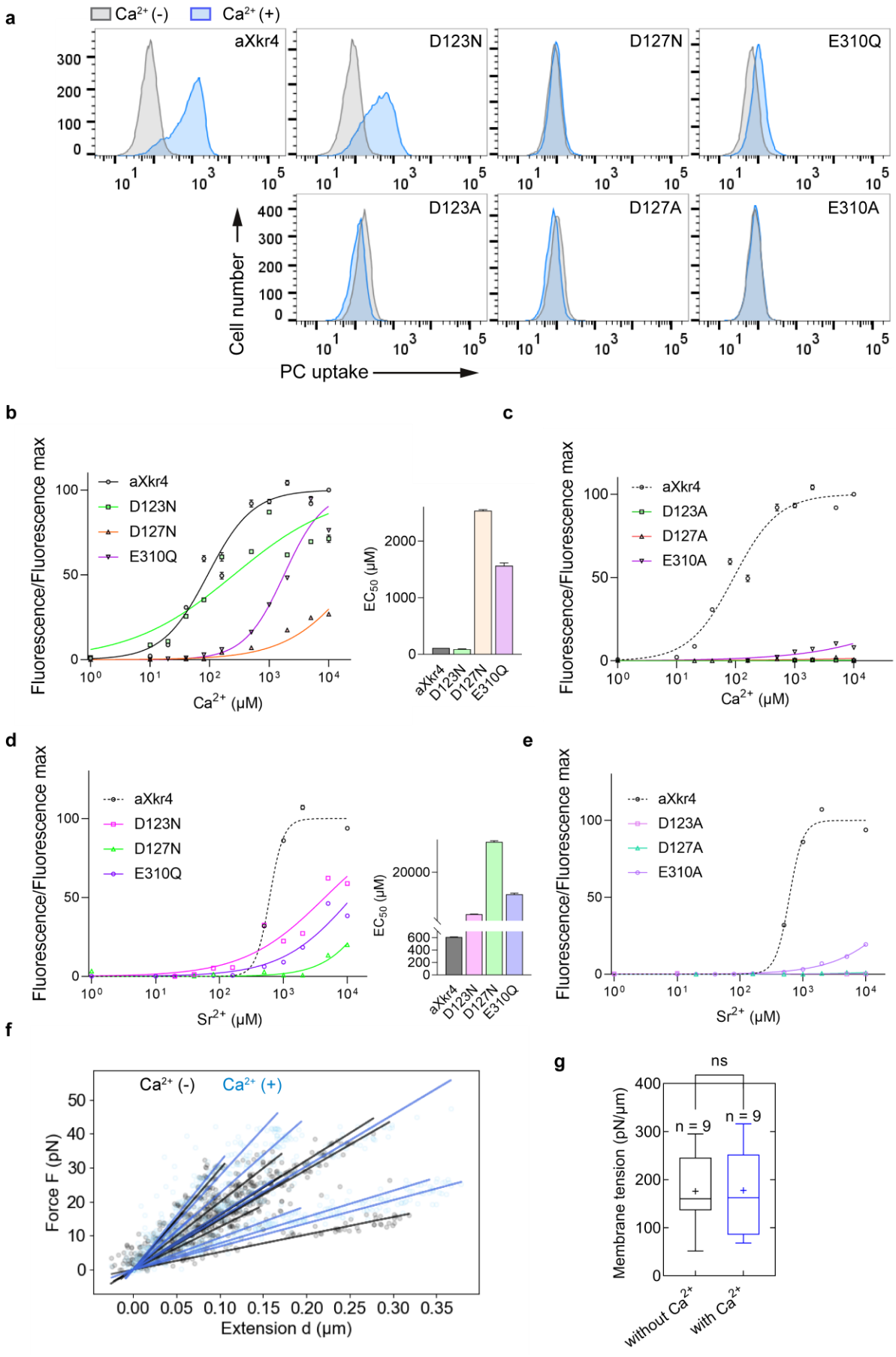
a
Ca2+ (-)
Ca2+ (+)
aXkr4
D123N
D127N
E310Q
D123A
D127A
E310A
Cell number
PC uptake
b
Fluorescence/Fluorescence max
aXkr4
D123N
D127N
E310Q
Ca2+ (μM)
EC50 (μM)
c
D123A
D127A
E310A
d
Sr2+ (μM)
e
f
Force F (pN)
Extension d (μm)
g
ns
n = 9
Membrane tension (pN/μm)
without Ca2+
with Ca2+

Fig. 11: Examination of the candidate Ca^{2+}-binding sites a PLS activity of aXkr4 mutants of the candidate Ca^{2+}-binding sites. BDKO cells expressing aXkr4 and its mutants (D123N, D127N, E310Q, D123A, D127A, and E310A) were measured the PLS activity using NBD-PC in the presence of a final concentration of 0.125 mM Ca^{2+} or not. PLS activity was analyzed by FACS. **b-e** Dose-response curves of aXkr4 and its mutants. BDKO cells expressing aXkr4 and its mutants (D123N, D127N, E310Q, D123A, D127A, and E310A) were treated with different concentrations of Ca^{2+} (**b, c**) or Sr2+ (**d, e**), the PLS activity was measured using NBD-PC by FACS. EC50 was calculated and shown in the right panel of (**b, d**). each condition was performed for three times and shown with SD. **f, g** Membrane tension of aXkr4 E310A mutant. BDKO cells expressing aXkr4 E310A was using to measure the membrane tension with 5 mM Ca^{2+} (green) or without Ca^{2+}. The membrane tension was calculated from the linear fit of solid lines and shown as force-extension curve (**f**), Summary of the membrane tension was shown as box-plots (**g**). not significant. **, $p < 0.01$.

3.8 Screening of Ca^{2+}-associated residues

In general, Ca^{2+} interacts with 6 to 8 oxygen atoms in proteins to stabilize Ca^{2+} binding. To investigate whether other residues are involved in establishing a Ca^{2+}-binding site, I focused on the region around D123, D127, and E310 in the predicted Xkr4 structure. In this region, I found that side chains of T307 and S311 in TM3, and S339 in TM4, were oriented towards the Ca^{2+} binding site (Fig. 12a). To examine their effects, Ala mutants were generated. As a result, T307A, S311A, and S339A decreased the PLS activity (Fig. 12b). Notably, T307 and S339 are highly conserved in Xkr8 and Xkr9, and Ala mutants of these two residues, T307A and S339A, showed a more significant decrease in the affinity to Ca^{2+} compared to S311A (Fig. 12c and d). These results suggested that T307 and S311 in TM3 along with S339 in TM4 collaborate with D123 and D127 in TM1, and E310 in TM3, to generate a Ca^{2+}-binding site.

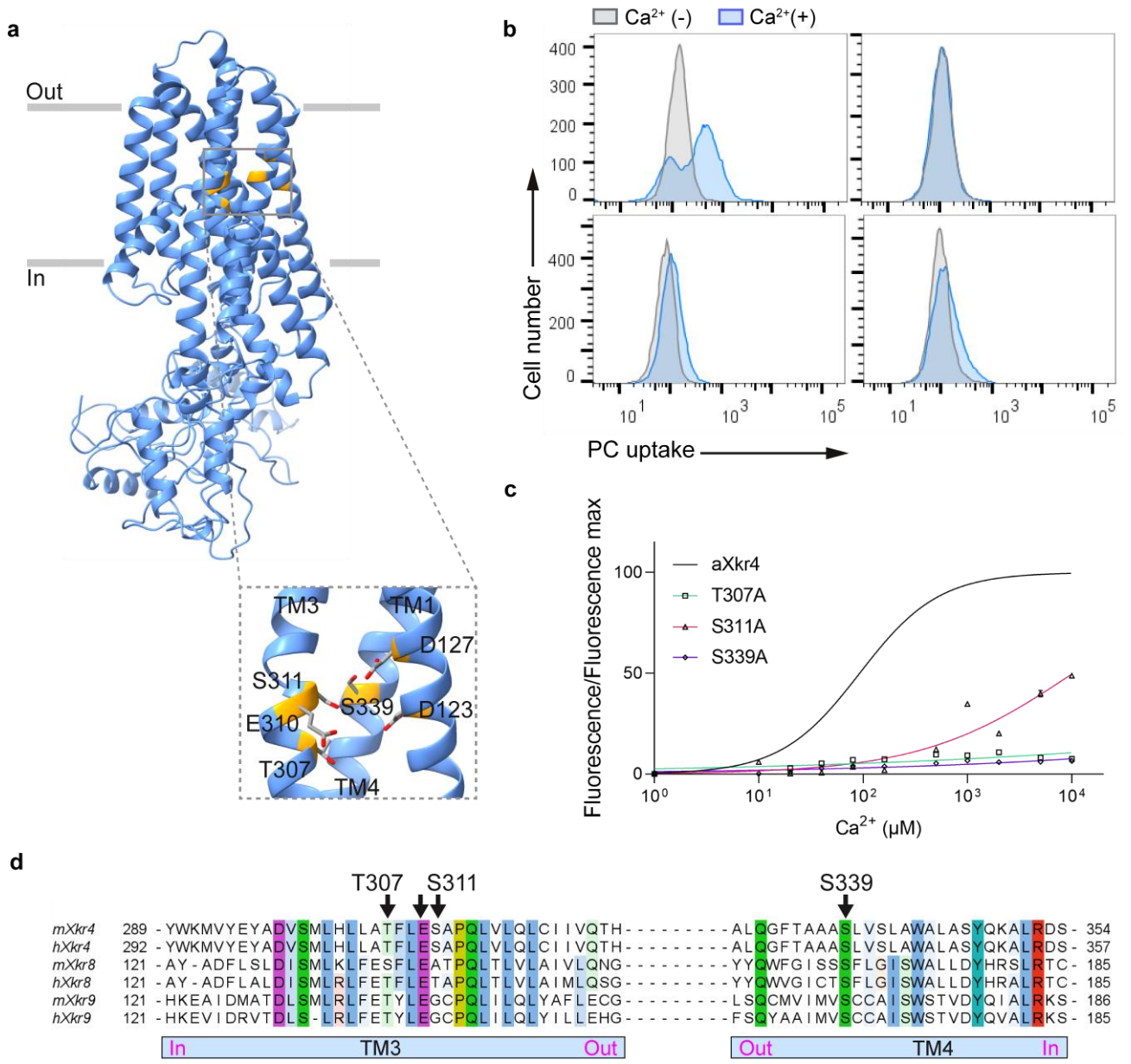

Fig. 12: Ca^{2+} binding sites of the non-charged residues a A view of Ca^{2+} binding site shown in Xkr4 structure. The Ca^{2+} binding sites of Xkr4 was highlighted in orange, and the residues were shown as sticks (oxygen: red). **b** PLS activity assay of aXkr4 and its mutants. BDKO cells expressing aXkr4 and its mutants (T307A, S311A, and S339A) were measured the PLS activity using NBD-PC in the presence of a final concentration of 0.125 mM Ca^{2+} or not. PLS activity was analyzed by FACS. **c** Dose-response curves of aXkr4 and its mutants. BDKO cells expressing aXkr4 and its mutants (T307A, S311A, and S339A) were treated with different concentrations of Ca^{2+} and the PLS activity was measured using NBD-PC by FACS. Each condition was performed for three times and shown as SD. **d** The sequence alignment of human and mouse Xkr4, Xkr8, and Xkr9. The sequence was colored according to the conserved, and the Ca^{2+} binding sites in TM3 and TM4 were highlighted with black arrow on the top of sequence based on the residue position of mXkr4.

3.9 Connection between transmembrane 1 and 3 by Ca^{2+}

Generally, Ca^{2+} binds to and activates proteins through the conformational changes. In the cases of TMEM16 family proteins, two Ca^{2+} connect TM6, TM7, and TM8, while an additional Ca^{2+} binds to TM2 and TM10 to facilitate the PLS activity[25,26,64]. Based on these findings, I hypothesized that Ca^{2+} serves as a "molecular glue" to connect TM1 and TM3 to activate Xkr family proteins. To examine the hypothesis, I performed a Cys scanning analysis in the Ca^{2+}-binding site to induce an artificial disulfide bond that bridges TM1 and TM3 (Fig. 13a and b). Amino acid residues from D123 to D127 in TM1 and E310 in TM3 were sequentially mutated into Cys. Treating with or without the oxidative reagent copper-phenanthroline (CuP)[65] did not alter the PLS activity (Fig. 13c and e). When Cys mutants in TM1 is generated in E310C background, strong PLS activity was observed in G125C/E310C-expressing cells after CuP treatment without Ca^{2+} (Fig. 13d, f, and g), demonstrating that the artificial disulfide bond formation between TM1 and TM3 activates PLS. Next, these Cys mutant-expressing cells were treated with iodine solution[66] to induce the disulfide bond formation. In consistent with CuP treatment, the Cys double mutant of G125C/E310C exhibited a high PLS activity after iodine treatment (Fig. 13h-j). Taken together, these results support our hypothesis that the activation of Xkr4 is driven by the connection between TM1 and TM3 though Ca^{2+} binding. To further confirm this, Arg and Lys mutations were inserted into Xkr4 to induce the salt bridge formation. Among several Arg and Lys mutants, the E310K mutant showed a significant PLS activity even in the absence of Ca^{2+}, while E310R triggered a slight PLS activity (Fig. 13k), supporting that Ca^{2+} activates the PLS activity of Xkr4 through the connection of TM1 and TM3. In summary, these findings provide strong evidence on our hypothesis that Ca^{2+} acts as a "molecular glue" to connect TM1 and TM3 through the Ca^{2+} binding site to activate Xkr family proteins.

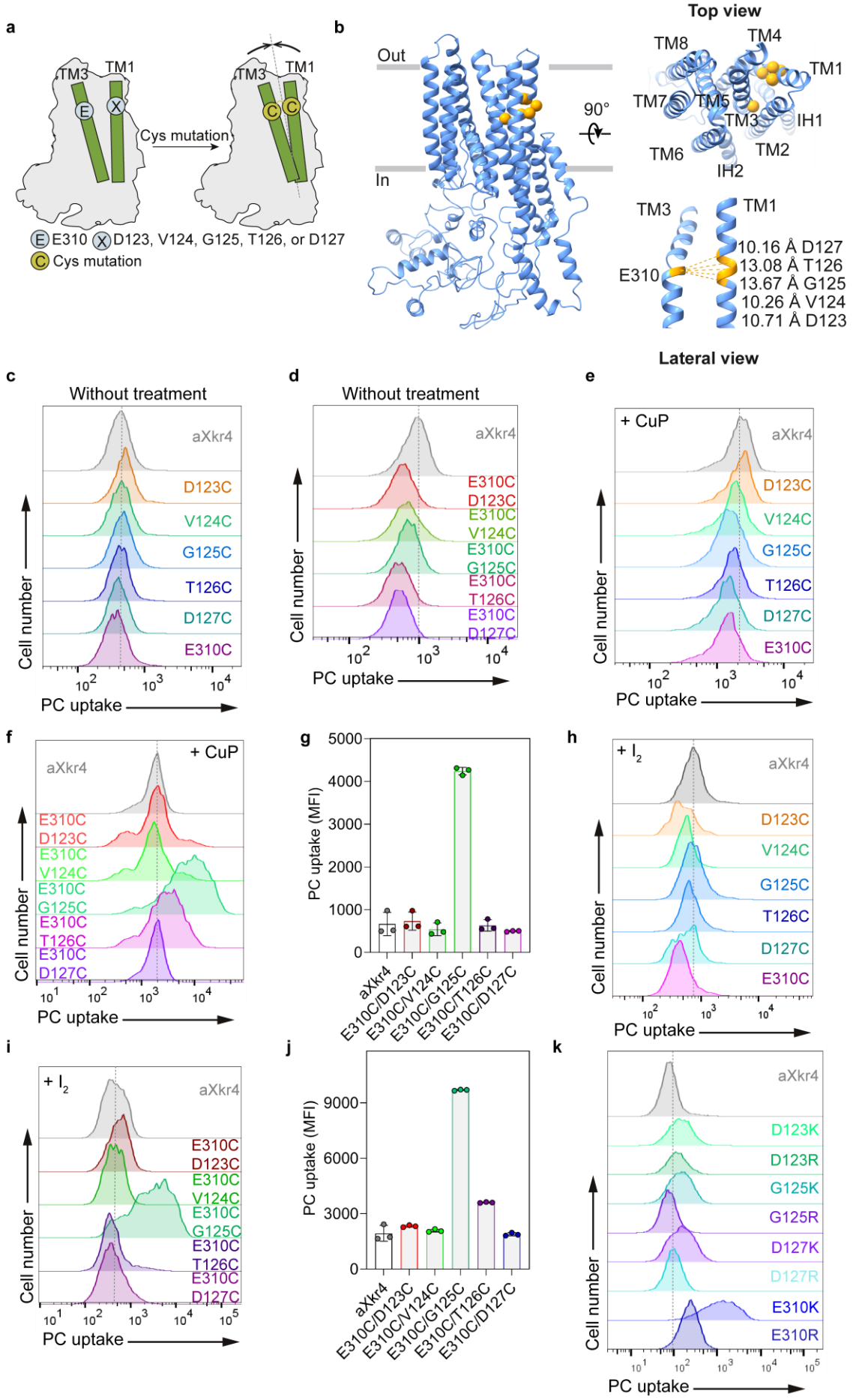
a
TM3
TM1
E
X
Cys mutation
C
E310 X D123, V124, G125, T126, or D127
C Cys mutation
b
Out
In
90°
Top view
TM8
TM4
TM1
TM7
TM5
TM3
IH1
TM6
TM2
IH2
TM3
TM1
E310
10.16 Å D127
13.08 Å T126
13.67 Å G125
10.26 Å V124
10.71 Å D123
Lateral view
c
Without treatment
aXkr4
D123C
V124C
G125C
T126C
D127C
E310C
Cell number
PC uptake
d
Without treatment
aXkr4
E310C
D123C
E310C
V124C
E310C
G125C
E310C
T126C
E310C
D127C
Cell number
PC uptake
e
+ CuP
aXkr4
D123C
V124C
G125C
T126C
D127C
E310C
Cell number
PC uptake
f
+ CuP
aXkr4
E310C
D123C
E310C
V124C
E310C
G125C
E310C
T126C
E310C
D127C
Cell number
PC uptake
g
PC uptake (MFI)
5000
4000
3000
2000
1000
0
aXkr4
E310C/D123C
E310C/V124C
E310C/G125C
E310C/T126C
E310C/D127C
h
+ I2
aXkr4
D123C
V124C
G125C
T126C
D127C
E310C
Cell number
PC uptake
i
+ I2
aXkr4
E310C
D123C
E310C
V124C
E310C
G125C
E310C
T126C
E310C
D127C
Cell number
PC uptake
j
PC uptake (MFI)
9000
6000
3000
0
aXkr4
E310C/D123C
E310C/V124C
E310C/G125C
E310C/T126C
E310C/D127C
k
aXkr4
D123K
D123R
G125K
G125R
D127K
D127R
E310K
E310R
Cell number
PC uptake

Fig. 13: Connection of TM1 and TM3 through Ca^{2+} binding a A Schematic model of Cys scanning in transmembrane domains of Xkr4. **b** Views of the Cys scanning sites of Xkr4. The Cys scanning sites are represented as yellow sphere at α carbon position of each residue, and the distances between E310 and the residues from D123 to D127 were described using the yellow dash lines. The Cys mutation sites in Xkr4 were viewed as top and lateral views. **c-j** PLS activity assay of aXkr4 and Cys mutants. BDKO cells expressing aXkr4 or Cys single mutants (**c, e, h**) or Cys double mutants (**d, f, i**) were measured the PLS activity using NBD-PC and analyzed by FACS. PLS activity of cells expressing aXkr4, Cys mutation, or Cys double mutations were analyzed without treatment as shown in (**c, d**). Cells expressing aXkr4, Cys mutation, or Cys double mutations were treated with CuP at a final concentration of 1.1 mM, incubated at room temperature for 20 min (**e, f**). or 25 μM iodine solution at room temperature for 10 min (**h, i**). PLS activity was analyzed by FACS. The triplicate data of PLS activity from the Cys double mutants were shown with SD, **g** for CuP treatment and j for iodine solution treatment. **k** the PLS activity of aXkr4 by Lys or Arg mutations. BDKO cells expressing aXkr4, Lys mutations or Arg mutations, were measured the PLS activity using NBD-PC without Ca^{2+}. The PLS activity was analyzed by FACS.

3.10 Molecular dynamics simulation of Ca^{2+} binding

To gain a deep understanding of how Ca^{2+} binding triggers the activation of Xkr4. A coarse-grained molecular dynamics (MD) simulation was performed using the predicted structure of aXkr4. In this model, the pseudo chemical bonds between pairs of the Ca^{2+} binding sites (D123 and D127 in TM1, and E310 in TM3) were created to mimic the Ca^{2+} binding in Xkr4. The simultaneous changes of movement of the amino acids in local regions was analyzed. Compared to the aXkr4 without the Ca^{2+} binding, significant changes of movement of the amino acids can be observed when the contact formation between TM1 and TM3 was simulated (Fig. 14a and b), indicating Ca^{2+} binding in TM1 and TM3 induces the conformational changes of Xkr4. These results further demonstrated that Ca^{2+} binding to TM1 and TM3 induces the conformational changes to activate the PLS activity of Xkr family proteins.

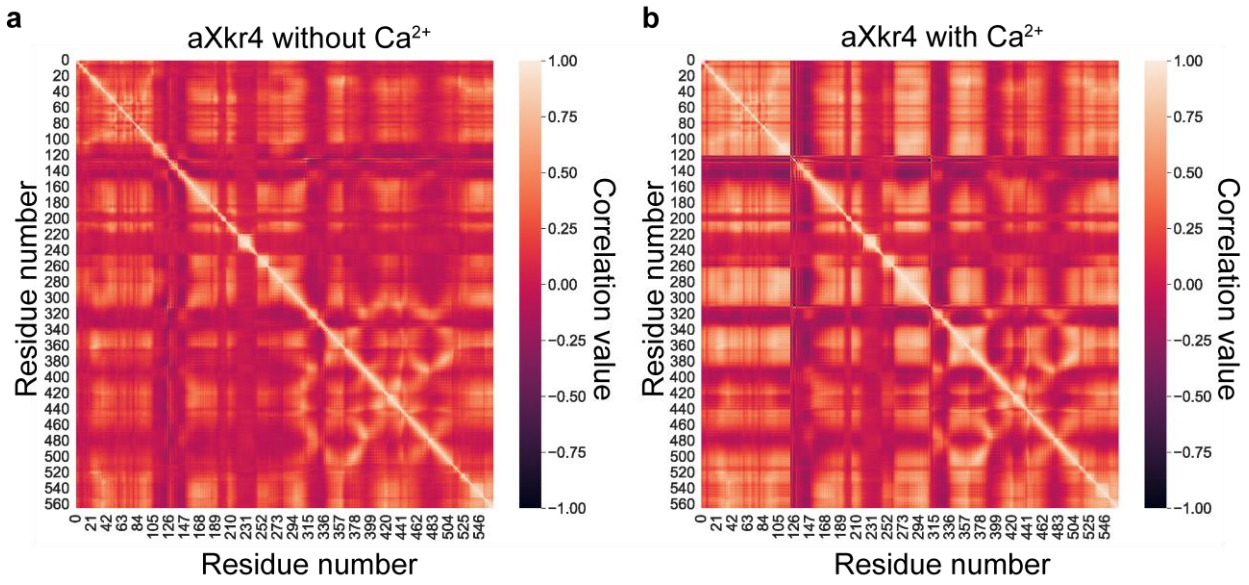

Fig. 14: Molecular dynamics simulation of Xkr4 with Ca^{2+} a, b Distance changes between each pair of amino acids were assessed via a correlation matrix after MD simulations and analyzed the trajectories. The distances between the Ca^{2+} position which is postulated to locate at the center of the Ca^{2+} binding sites (D123, D127, and E310) and other amino acids were calculated. **a** Correlation matrix of aXkr4 without Ca^{2+}. **b** Correlation matrix of aXkr4 with Ca^{2+} bridge. To mimic Ca^{2+} binding, we applied " Ca^{2+} bridge".

3.11 Thermostability of Xkr4 with Ca^{2+}

The binding of Ca^{2+} induces conformational changes in Xkr4 by the rearrangement of TM1 and TM3. Next, we asked the timing in which Ca^{2+} binds to Xkr4. To examine this, I investigated whether Ca^{2+} binding to Xkr4 has an impact on the stability of Xkr4. I transiently expressed Xkr4ΔC and aXkr4 tagged with an EGFP at C-terminus in HEK293T cells. Whole cell lysate was prepared using a detergent combination of Glyco-dendrimer (GDN) and Lauryl Maltose Neopentyl Glycol (LMNG) at a ratio of 1:1, and a dimer fraction was collected using size exclusion chromatography (SEC). The protein thermostability was examined by incubating collected proteins at various temperatures with Ca^{2+} or EGTA. As shown in the Fig. 15a-d, aXkr4, but not Xkr4ΔC, dimer showed a decrease in thermostability in the absence of Ca^{2+} compared to that in the presence of Ca^{2+}: dimers were dissociated into monomers at higher temperatures. These results suggested that Ca^{2+} binding occurs when Xkr4 is transitioned into a pre-activated state such as aXkr4.

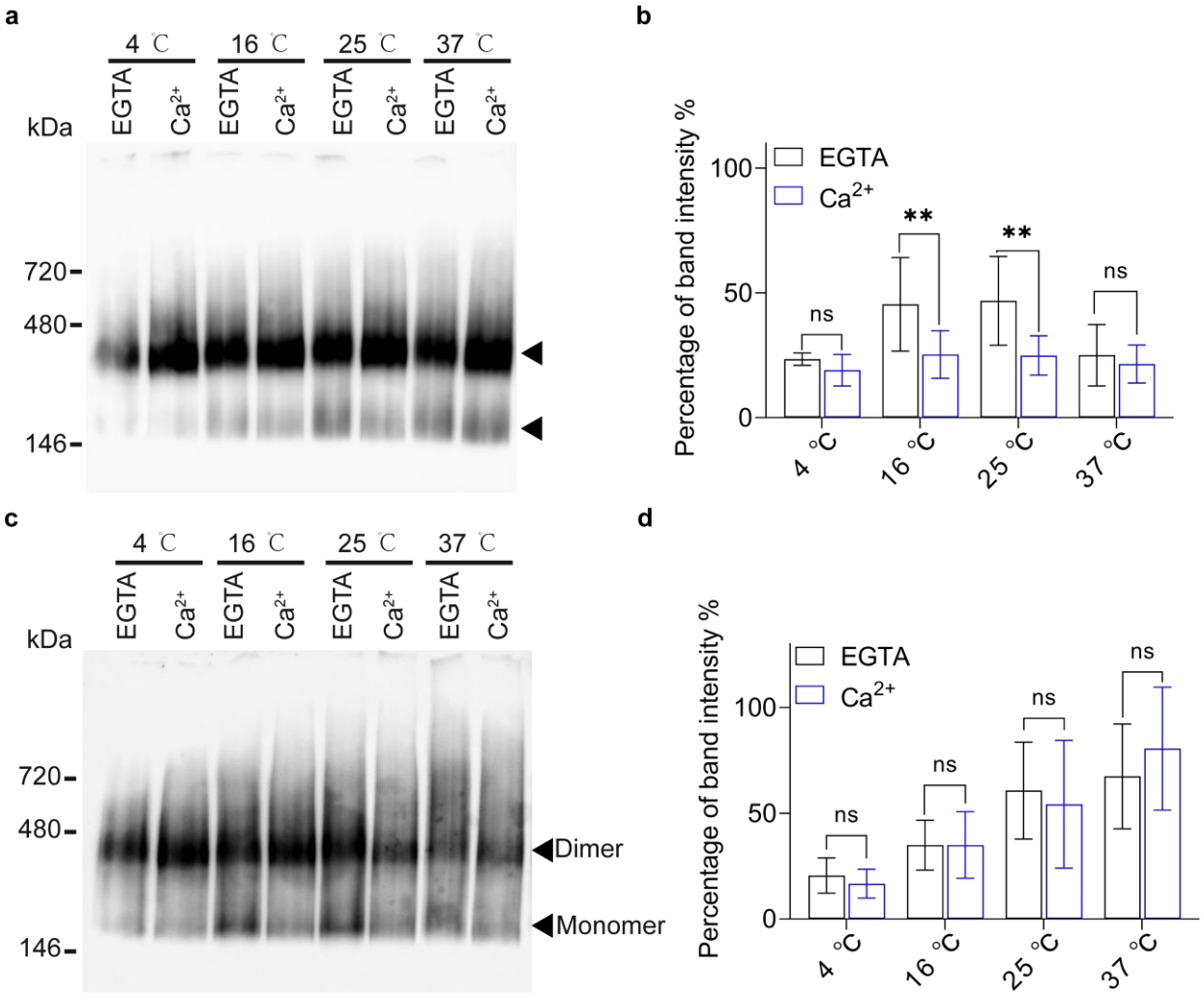

Fig. 15: Thermostability of Xkr4 a-d mXkr4ΔC (**a, b**) or aXkr4 (**c, d**) were transiently expressed in HEK293T cells. The whole cell lysate was prepared using 0.5% GDN and 0.5% LMNG in the presence of 1 mM Ca^{2+} or 0.5 mM EGTA. The dimer of mXkr4ΔC or aXkr4 were separated from monomer and collected using size exclusion chromatography, and analyzed by BN-PAGE. mXkr4ΔC and aXkr4 were detected by anti-V5 antibody. BN-PAGE analysis of each was performed for three times, and the images was analyzed using ImageJ software. The total amount of proteins including dimer and monomer before incubation was defined as 100%. The percentage of monomers was shown in histogram with SD (**b, d**). ns, not significant. **, $p < 0.01$.

3.12 Activation model of Xkr4

Next, I aimed to understand whether the connection of TM1 and TM3 alone is able to induce the PLS activity of Xkr4. To examine this, I introduced Cys double mutations G125C/E310C into both Xkr4FL and Xkr4ΔC, and induced the disulfide bond through the CuP or I_2 treatment. Xkr4FL was unable to induce the PLS activity, and Xkr4ΔC exhibited a slight PLS activity by the artificial disulfide bond formation but lower than that of aXkr4 G125C/E310C (Fig. 16a-c). These results suggested that

XRCC4/C binding to Xkr4ΔC plays an essential role for the Ca^{2+}-mediated activation of the Xkr4 dimer. Indeed, introduction of XRCC4/C into Xkr4ΔC G125C/E310C-expressing cells activated the PLS activity after treating with CuP or I_2 (Fig. 16d and e). In the case of salt bridge formation, insertion of the E310K mutation into both Xkr4FL and Xkr4ΔC failed to activate the PLS activity unlike aXkr4 E310K (Fig. 16f), further demonstrating that the connection between TM1 and TM3 induced the PLC activity in a pre-activated state. Based on these findings, I hypothesized a novel activation model of Xkr4: 1. Caspase-mediated cleavage of Xkr4 triggers dimer formation; 2. The caspase-cleaved fragment of XRCC4 binds to the Xkr4 dimer to prepare for activation; 3. Extracellular Ca^{2+} binds to and connects the TM1 and TM3 to induce the conformation changes for Xkr4 activation (Fig. 16h and i).

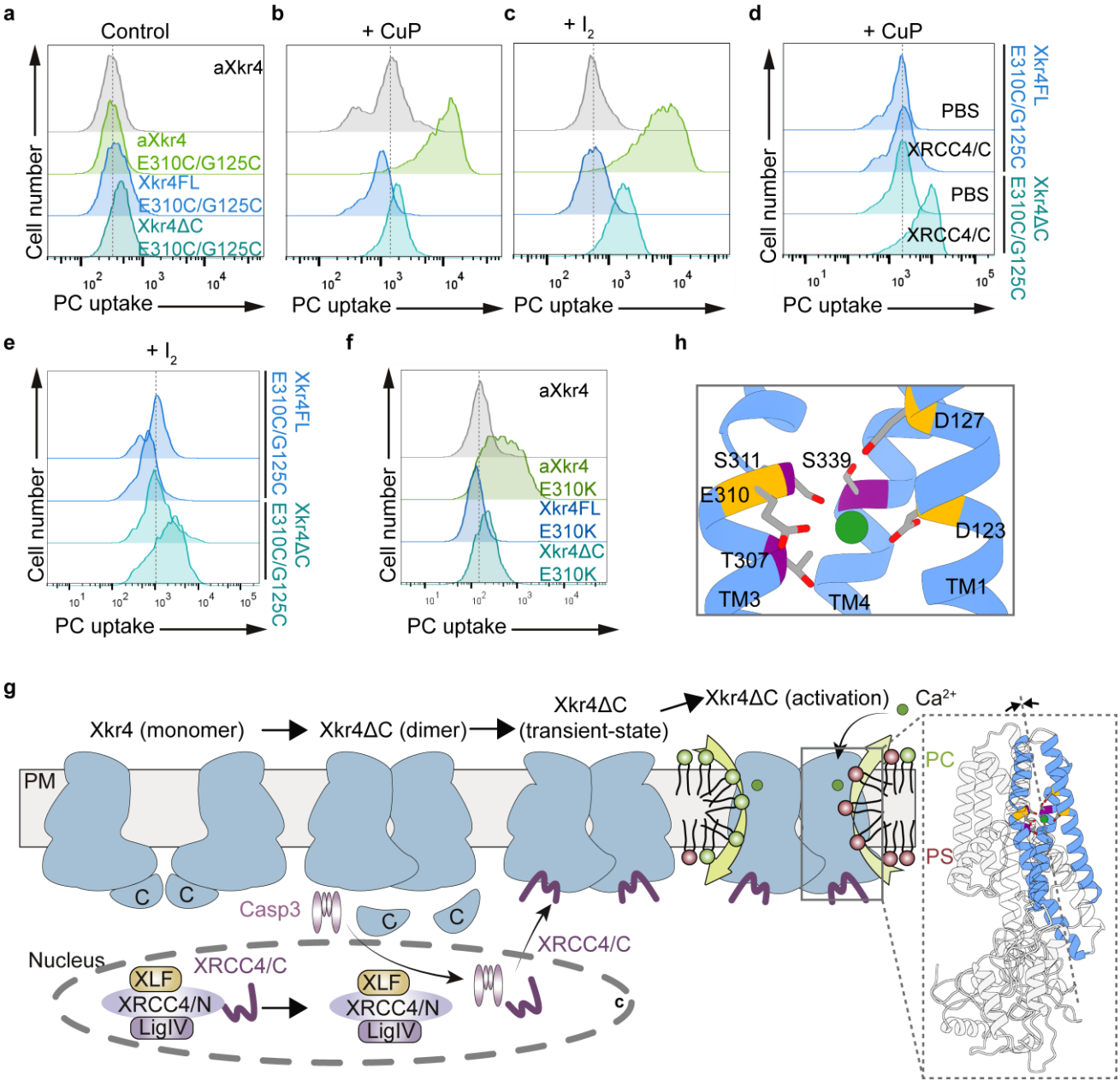

Fig. 16: Activation mechanism of Xkr4 a-f Activation of Cys double mutations of different types of Xkr4. Xkr4FL, Xkr4ΔC, or aXkr4 with G125C/E310C mutations and aXkr4 (**a**) were expressed in BDKO cells, and BDKO cells were incubated with 1.1 mM CuP at a final concentration at room temperature for 20 min (**b**), or 25 μM iodine solution at a final concentration at room temperature for 10 min (**c**), PLS activity was measured using NBD-PC and analyzed by FACS. BDKO cells expressing aXkr4, Xkr4FL, or Xkr4ΔC G125C/E310C were introduced XRCC4/C by electroporation at 0.5 μM, and PBS was used as control, and follow were treated with 1.1 mM CuP (**d**) or 25 μM iodine solution (**e**), PLS activity was measured using NBD-PC and analyzed by FACS. BDKO cells expressing aXkr4, Xkr4FL E310K, or Xkr4ΔC E310K were introduced XRCC4/C by electroporation at 0.5 μM. PLS activity was measured using NBD-PC, and analyzed by FACS. **f** Xkr4 activation in Lys mutation. BDKO cells expressing aXkr4, aXkr4 E310K, Xkr4FL E310K, or Xkr4ΔC E310K were applied to the PLS assay without Ca^{2+}. **g** The activation model of Xkr4. The C-terminus of Xkr4 was cleaved by caspase3 (Casp3), and form a homodimer. XRCC4/C binds to Xkr4 dimer after cleavage by Casp3. The Ca^{2+} binding sites of Xkr4 were shown as sticks (oxygen: red). The negatively-charged residues (D123, D127, E310) were colored as orange, and the non-charged residues (T307, S311, S339) were colored as purple. Lime green circle, Ca^{2+}. XRCC4/N, N-terminus of XRCC4. LigIV, DNA ligaseIV. **h** a close-up view of Ca^{2+} binding sites.

4. Discussion

Within the Xkr family, Xkr4, Xkr8, and Xkr9 are caspase-mediated dependent scramblases. Xkr8 is activated through dimerization by caspase-mediated cleavage of C-terminus Similarly, Xkr4 is dimerized by caspase-mediated cleavage, but the dimerization alone is insufficient for activation. In the case of Xkr4, the nucleus protein XRCC4 is required. In this study, I found that a direct binding of the XRCC4 fragment is necessary to induce the Xkr4 PLS activity, but not fully activate Xkr4. Our finding proved that the extracellular Ca^{2+} is additionally required to activate Xkr4, Xkr8, and Xkr9. Through Ala scanning, I discovered that the conserved negatively-charged residues among the Xkr family members, D123 and D127 in TM1 and E310 in TM3 of Xkr4, coordinated a Ca^{2+} binding stie. These amino acid residues also associated with T307 and S311 in TM3 and S339 in TM4 to coordinate the Ca^{2+} binding site, suggesting that Ca^{2+} binding induces the conformational changes.

4.1 Activation of Xkr4 by XRCC4

XRCC4 is a nuclear protein that is related to the DNA repair. The C-terminus of XRCC4 is cleaved by caspase and directly binds to and activate Xkr4 on the plasma membranes. Analysis of the XRCC4 C-terminus showed that the region consists of an intrinsically disordered regions, generally involved in liquid-liquid phase separation (LLPS). It would be interesting whether LLPS is linked to the regulation of XRCC4 for Xkr4 activation. Furthermore, Xkr4 is specifically expressed in brain, suggesting a significant role of XRCC4-mediated Xkr4 activation in brain function. It is known that neuronal activity regulates not only rapid gene expression accompanying a DNA double-strand breaks but also synapse elimination[67–71]. Therefore, it would be intriguing to investigate the potential connection between the activity-dependent DNA damage pathway and synaptic elimination mediated by the XRCC4 fragment.

4.2 Activation of Xkr4 by Ca^{2+}

Ca^{2+} predominantly interacts with oxygen atoms of carboxyl side chains of Asp, Glu, Asn, and Gln, as well as hydroxyl group of Ser and Thr[72], and water. So far, the EF hand motif, characterized by a helix-loop-helix, has been the most common motif for specifically interacting with Ca^{2+} and revealing a conserved pattern of DxDxD in the loop domain[73]. The domain is flexible and allows proteins to undergo conformational changes in respond to Ca^{2+} binding. In contrast, Ca^{2+} binds to the

transmembrane region in the TMEM16 family proteins, in which most of them serve as a scramblase[22]. Each TMEM16 molecule contains two distinct Ca^{2+}-binding sites. One of them is located in TM6, TM7, and TM8, while the other is located in TM2 and TM10. Ca^{2+} binding to TMEM16 proteins induce a conformational change in the embedded hydrophilic groove, composed of TM4 and TM6, to expose the groove for phospholipid heap translocation[25,26,30]. In this study, I have discovered that Ca^{2+} also binds to the transmembrane region of Xkr family proteins, a caspase-dependent scramblase. My hypothesis is that Ca^{2+} binding triggers the conformational change of Xkr proteins similar to TMEM16F protein to expose the hydrophilic groove. It is possible that Ca^{2+} binding to the transmembrane region is shared mechanisms in multiple scramblases to create the phospholipid transfer pathway.

In the Xkr family, the Nagata and Dutzler groups have solved the monomeric structures of Xkr8 and Xkr9, respectively[36,37]. The predicted structure of Xkr4 is highly similar to Xkr8 and Xkr9, especially for the transmembrane region (Fig. 10d). Furthermore, the two groups proposed the potential phospholipid translocation pathways in Xkr8 and Xkr9, and highlighted an important role of TM3 to induce the PLS activity of Xkr family. TM3 contains highly conserved hydrophilic residues including polar and charged amino acids, and I found that T307, E310, and S311 in TM3, and D123 and D127 in TM1, and S339 in TM4 were coordinated with Ca^{2+} to induce the PLS activity. Introducing an artificial disulfide bond or a salt bridge in the Ca^{2+} binding sites, was successful in activating the PLS activity of Xkr4 (Fig. 13f, i, and k), suggesting that Ca^{2+} binding functions as a “molecular glue” and bridges TM1 and TM3. Using MD simulation, I compared the structural changes of aXkr4 with or without Ca^{2+} binding, and the results demonstrated that Ca^{2+} binding in TM1 and TM3 caused the conformational changes (Fig. 14a and b). Taking together, these results suggest that Ca^{2+} binding connects TM1 and TM3, and then induces conformational changes in Xkr4 to induce the PLS activity. The details of the conformational changes occurring when Xkr4 binds with XRCC4/C and Ca^{2+} need to be the figured out through the structure analyses such as Cryo-EM and X-ray analyses. However, it is worth noting that performing structure analysis of Xkr dimers is still a big challenge in the field, as the purified Xkr dimer tends to be unstable and aggregated (Fig. 17a to f). Overcoming these problems will be a significant breakthrough for structure analysis in the future.

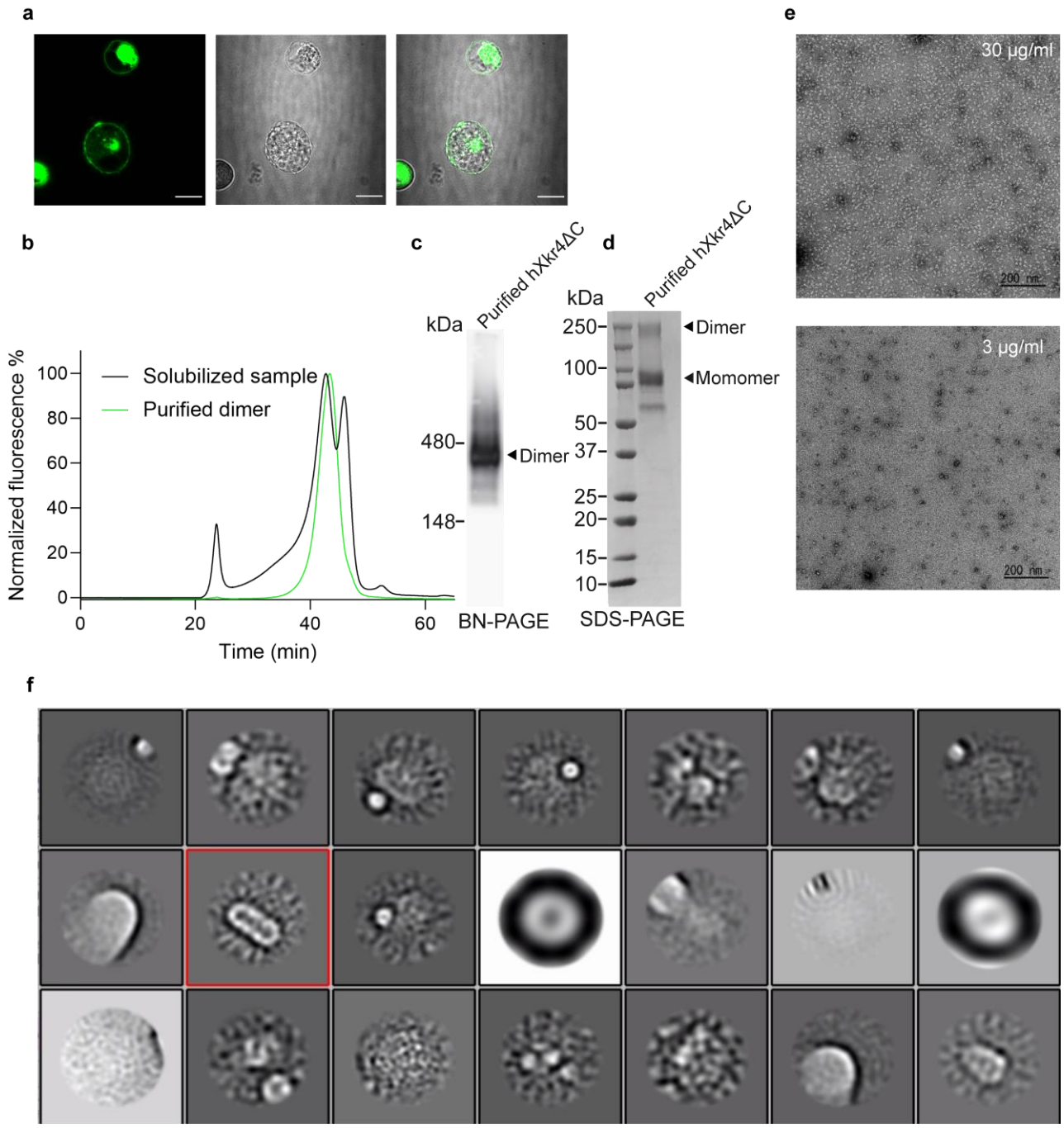

Fig. 17: Cryo-EM structure analysis of human Xkr4ΔC (hXkr4ΔC) **a** Expression and localization of hXkr4ΔC fused with monomeric GFP in FS293F cells. scale bare: 20 μm. **b-d** Size exclusion chromatography (SEC) of hXkr4ΔC. The hXkr4ΔC, purified by affinity purification using nickel column, was applied to SEC and the dimer peak was collected at 39 to 44 min (left, black). Collected dimer was applied to SEC (**b**) and BN-PAGE, followed by detection with anti-V5 antibody (**c**) or SDS-gel staining by CBB (**d**). **e** Negative staining of purified hXkr4 dimer. Negative staining reflects the homogeneity of purified Xkr4 dimer. Purified Xkr4 was diluted to 30 μg/ml (upper) and 3 μg/ml (lower). **f** A representative two-dimensional image. A high-quality two-dimensional image was highlighted by a red square.

Compared to Xkr8 expressing in all tissues, Xkr4 shows a tissue-specific expression in the brain[13],

where PS exposure plays a role in eliminating the unwanted synapses in living neurons[70,71,74]. It is widely known that extracellular Ca^{2+} is incorporated by activated synapse to regulate neuronal function[75,76]. Given the limited size and constrained access to the synaptic cleft, it is hypothesized that the influx of Ca^{2+} from both presynaptic and postsynaptic regions during neurotransmission could significantly reduce Ca^{2+} concentrations within the synaptic cleft, possibly dropping as low as 0.3 mM[77–81]. Although actual measurements are essential, if extracellular Ca^{2+} levels decrease to less than 0.3 mM at the active synapse, it could potentially inhibit Xkr4 activation more effectively, and prevent the engulfment of the active synapse. A recent study reported that Xkr8 is involved in the axon pruning through the PS exposure[82]. Considering the neuron-specific expression of Xkr4, it will be interesting to reveal the physiological roles of Xkr4 in the neuron regulation.

In summary, the results suggest that XRCC4/C activates Xkr4 in direct binding manner, and the extracellular Ca^{2+} plays a critical role for the activation of Xkr4, Xkr8, and Xkr9, by binding and connecting the TM1 and TM3, which XRCC4/C binding to Xkr4 provides an intermediate state for Ca^{2+} binding. These findings will be contributing to understanding the mechanism of Xkr4 and other scramblases.

5. Bibliography

1. Harayama, T. & Riezman, H. Understanding the diversity of membrane lipid composition. *Nat Rev Mol Cell Biol* **19**, 281–296 (2018).
2. Vance, J. E. Phospholipid Synthesis and Transport in Mammalian Cells. *Traffic* **16**, 1–18 (2015).
3. van Meer, G., Voelker, D. R. & Feigenson, G. W. Membrane lipids: where they are and how they behave. *Nat Rev Mol Cell Biol* **9**, 112–124 (2008).
4. Leventis, P. A. & Grinstein, S. The Distribution and Function of Phosphatidylserine in Cellular Membranes. *Annual Review of Biophysics* **39**, 407–427 (2010).
5. Andersen, J. P. *et al.* P4-ATPases as Phospholipid Flippases—Structure, Function, and Enigmas. *Frontiers in Physiology* **7**, (2016).
6. Zwaal, R. F. A., Comfurius, P. & Bevers, E. M. Surface exposure of phosphatidylserine in pathological cells. *CMLS, Cell. Mol. Life Sci.* **62**, 971–988 (2005).
7. Nagata, S. Apoptosis and Clearance of Apoptotic Cells. *Annual Review of Immunology* **36**, 489–517 (2018).
8. Ravichandran, K. S. Find-me and eat-me signals in apoptotic cell clearance: progress and conundrums. *Journal of Experimental Medicine* **207**, 1807–1817 (2010).
9. Bevers, E. M. & Williamson, P. L. Getting to the Outer Leaflet: Physiology of Phosphatidylserine Exposure at the Plasma Membrane. *Physiological Reviews* **96**, 605–645 (2016).
10. Nagata, S., Sakuragi, T. & Segawa, K. Flippase and scramblase for phosphatidylserine exposure. *Current Opinion in Immunology* **62**, 31–38 (2020).
11. Pomorski, T. & Menon, A. K. Lipid flippases and their biological functions. *Cell. Mol. Life Sci.* **63**, 2908–2921 (2006).
12. Suzuki, J. *et al.* Calcium-dependent Phospholipid Scramblase Activity of TMEM16 Protein Family Members. *Journal of Biological Chemistry* **288**, 13305–13316 (2013).
13. Suzuki, J., Imanishi, E. & Nagata, S. Exposure of Phosphatidylserine by Xk-related Protein Family

Members during Apoptosis. *Journal of Biological Chemistry* **289**, 30257–30267 (2014).

14. Suzuki, J., Umeda, M., Sims, P. J. & Nagata, S. Calcium-dependent phospholipid scrambling by TMEM16F. *Nature* **468**, 834–838 (2010).
15. Suzuki, J., Denning, D. P., Imanishi, E., Horvitz, H. R. & Nagata, S. Xk-Related Protein 8 and CED-8 Promote Phosphatidylserine Exposure in Apoptotic Cells. *Science* **341**, 403–406 (2013).
16. Lee, B.-C. *et al.* Gating mechanism of the extracellular entry to the lipid pathway in a TMEM16 scramblase. *Nature Communications* **9**, 3251 (2018).
17. Watanabe, R., Sakuragi, T., Noji, H. & Nagata, S. Single-molecule analysis of phospholipid scrambling by TMEM16F. *Proceedings of the National Academy of Sciences* **115**, 3066–3071 (2018).
18. Caputo, A. *et al.* TMEM16A, A Membrane Protein Associated with Calcium-Dependent Chloride Channel Activity. *Science* **322**, 590–594 (2008).
19. Yang, Y. D. *et al.* TMEM16A confers receptor-activated calcium-dependent chloride conductance. *Nature* **455**, 1210–1215 (2008).
20. Schroeder, B. C., Cheng, T., Jan, Y. N. & Jan, L. Y. Expression Cloning of TMEM16A as a Calcium-Activated Chloride Channel Subunit. *Cell* **134**, 1019–1029 (2008).
21. Gyobu, S., Ishihara, K., Suzuki, J., Segawa, K. & Nagata, S. Characterization of the scrambling domain of the TMEM16 family. *Proceedings of the National Academy of Sciences* **114**, 6274–6279 (2017).
22. Suzuki, J. *et al.* Calcium-dependent Phospholipid Scramblase Activity of TMEM16 Protein Family Members. *Journal of Biological Chemistry* **288**, 13305–13316 (2013).
23. Maruoka, M. & Suzuki, J. Regulation of phospholipid dynamics in brain. *Neuroscience Research* **167**, 30–37 (2021).
24. Dang, S. *et al.* Cryo-EM structures of the TMEM16A calcium-activated chloride channel. *Nature* **552**, 426–429 (2017).

25. Alvadia, C. *et al.* Cryo-EM structures and functional characterization of the murine lipid scramblase TMEM16F. *eLife* **8**, e44365 (2019).
26. Bushell, S. R. *et al.* The structural basis of lipid scrambling and inactivation in the endoplasmic reticulum scramblase TMEM16K. *Nat Commun* **10**, 3956 (2019).
27. Falzone, M. E. *et al.* Structural basis of Ca2+-dependent activation and lipid transport by a TMEM16 scramblase. *eLife* **8**, e43229 (2019).
28. Brunner, J. D., Lim, N. K., Schenck, S., Duerst, A. & Dutzler, R. X-ray structure of a calcium-activated TMEM16 lipid scramblase. *Nature* **516**, 207–212 (2014).
29. Kalienkova, V. *et al.* Stepwise activation mechanism of the scramblase nhTMEM16 revealed by cryo-EM. *eLife* **8**, e44364 (2019).
30. Le, S. C. & Yang, H. An Additional Ca2+ Binding Site Allosterically Controls TMEM16A Activation. *Cell Reports* **33**, 108570 (2020).
31. Feng, S. *et al.* Cryo-EM Studies of TMEM16F Calcium-Activated Ion Channel Suggest Features Important for Lipid Scrambling. *Cell Reports* **28**, 567-579.e4 (2019).
32. Khelashvili, G. *et al.* Dynamic modulation of the lipid translocation groove generates a conductive ion channel in Ca2+-bound nhTMEM16. *Nat Commun* **10**, 4972 (2019).
33. Falzone, M. E. *et al.* TMEM16 scramblases thin the membrane to enable lipid scrambling. *Nat Commun* **13**, 2604 (2022).
34. Arndt, M. *et al.* Structural basis for the activation of the lipid scramblase TMEM16F. *Nat Commun* **13**, 6692 (2022).
35. Suzuki, J., Imanishi, E. & Nagata, S. Xkr8 phospholipid scrambling complex in apoptotic phosphatidylserine exposure. *Proceedings of the National Academy of Sciences* **113**, 9509–9514 (2016).
36. Straub, M. S., Alvadia, C., Sawicka, M. & Dutzler, R. Cryo-EM structures of the caspase-activated protein XKR9 involved in apoptotic lipid scrambling. *eLife* **10**, e69800 (2021).

37. Sakuragi, T. *et al.* The tertiary structure of the human Xkr8–Basigin complex that scrambles phospholipids at plasma membranes. *Nat Struct Mol Biol* **28**, 825–834 (2021).
38. Sakahira, H., Enari, M. & Nagata, S. Cleavage of CAD inhibitor in CAD activation and DNA degradation during apoptosis. *Nature* **391**, 96–99 (1998).
39. Maruoka, M. *et al.* Caspase cleavage releases a nuclear protein fragment that stimulates phospholipid scrambling at the plasma membrane. *Molecular Cell* **81**, 1397-1410.e9 (2021).
40. Ahnesorg, P., Smith, P. & Jackson, S. P. XLF Interacts with the XRCC4-DNA Ligase IV Complex to Promote DNA Nonhomologous End-Joining. *Cell* **124**, 301–313 (2006).
41. Chang, H. H. Y., Pannunzio, N. R., Adachi, N. & Lieber, M. R. Non-homologous DNA end joining and alternative pathways to double-strand break repair. *Nat Rev Mol Cell Biol* **18**, 495–506 (2017).
42. Ryoden, Y., Segawa, K. & Nagata, S. Requirement of Xk and Vps13a for the P2X7-mediated phospholipid scrambling and cell lysis in mouse T cells. *Proc. Natl. Acad. Sci. U.S.A.* **119**, e2119286119 (2022).
43. Guillén-Samander, A. *et al.* A partnership between the lipid scramblase XK and the lipid transfer protein VPS13A at the plasma membrane. *Proceedings of the National Academy of Sciences* **119**, e2205425119 (2022).
44. Yoshida, H. *et al.* Phosphatidylserine-dependent engulfment by macrophages of nuclei from erythroid precursor cells. *Nature* **437**, 754–758 (2005).
45. Schneider, C. A., Rasband, W. S. & Eliceiri, K. W. NIH Image to ImageJ: 25 years of image analysis. *Nat Methods* **9**, 671–675 (2012).
46. Waterhouse, A. M., Procter, J. B., Martin, D. M. A., Clamp, M. & Barton, G. J. Jalview Version 2--a multiple sequence alignment editor and analysis workbench. *Bioinformatics* **25**, 1189–1191 (2009).
47. Hunter, John D. "Matplotlib: A 2D graphics environment." Computing in science & engineering 9 (2007): 90-95

48. Harris, C. R. *et al.* Array programming with NumPy. *Nature* **585**, 357–362 (2020).
49. Sánchez, R. & Šali, A. Evaluation of comparative protein structure modeling by MODELLER-3. *Proteins: Structure, Function, and Bioinformatics* **29**, 50–58 (1997).
50. Baek, M. *et al.* Accurate prediction of protein structures and interactions using a three-track neural network. *Science* **373**, 871–876 (2021).
51. Palacios, R. & Steinmetz, M. IL3-dependent mouse clones that express B-220 surface antigen, contain ig genes in germ-line configuration, and generate B lymphocytes in vivo. *Cell* **41**, 727–734 (1985).
52. Fukunaga, R., Ishizaka-Ikeda, E. & Nagata, S. Purification and characterization of the receptor for murine granulocyte colony-stimulating factor. *Journal of Biological Chemistry* **265**, 14008–14015 (1990).
53. Tucker, Kent A., et al. Characterization of a new human diploid myeloid leukemia cell line (PLB-985) with granulocytic and monocytic differentiating capacity. Blood 70, 372-378 (1987).
54. Hanayama, R. *et al.* Identification of a factor that links apoptotic cells to phagocytes. *Nature* **417**, 182–187 (2002).
55. Tsuchiya, M. *et al.* Cell surface flip-flop of phosphatidylserine is critical for PIEZO1-mediated myotube formation. *Nat Commun* **9**, 2049 (2018).
56. Kenzaki, H. *et al.* CafeMol: A Coarse-Grained Biomolecular Simulator for Simulating Proteins at Work. *J. Chem. Theory Comput.* **7**, 1979–1989 (2011).
57. Li, Z. *et al.* The XRCC4 gene encodes a novel protein involved in DNA double-strand break repair and V(D)J recombination. *Cell* **83**, 1079–1089 (1995).
58. Shiomi, A. *et al.* Extreme deformability of insect cell membranes is governed by phospholipid scrambling. *Cell Reports* **35**, 109219 (2021).
59. Dudev, T. & Lim, C. Competition among Metal Ions for Protein Binding Sites: Determinants of Metal Ion Selectivity in Proteins. *Chem. Rev.* **114**, 538–556 (2014).

60. Kumarevel, T. Characterization of the metal ion binding site in the anti-terminator protein, HutP, of Bacillus subtilis. *Nucleic Acids Research* **33**, 5494–5502 (2005).

61. Gupta, S. K. *et al.* Luminescence Properties of $SrZrO_3/Tb^{3+}$ Perovskite: Host-Dopant Energy-Transfer Dynamics and Local Structure of Tb3+. *Inorg. Chem.* **55**, 1728–1740 (2016).

62. Cheng, W. *et al.* Selective removal of divalent cations by polyelectrolyte multilayer nanofiltration membrane: Role of polyelectrolyte charge, ion size, and ionic strength. *Journal of Membrane Science* **559**, 98–106 (2018).

63. Ishihara, K., Suzuki, J. & Nagata, S. Role of Ca^{2+} in the Stability and Function of TMEM16F and 16K. *Biochemistry* **55**, 3180–3188 (2016).

64. Khelashvili, G. & Menon, A. K. Phospholipid Scrambling by G Protein–Coupled Receptors. *Annual Review of Biophysics* **51**, 39–61 (2022).

65. Xue, L. *et al.* Rearrangement of the transmembrane domain interfaces associated with the activation of a GPCR hetero-oligomer. *Nat Commun* **10**, 2765 (2019).

66. Zhou, Y., Ramachandran, S., Oh-hora, M., Rao, A. & Hogan, P. G. Pore architecture of the ORAI1 store-operated calcium channel. *Proc. Natl. Acad. Sci. U.S.A.* **107**, 4896–4901 (2010).

67. Stevens, B. *et al.* The Classical Complement Cascade Mediates CNS Synapse Elimination. *Cell* **131**, 1164–1178 (2007).

68. Chung, W.-S. *et al.* Astrocytes mediate synapse elimination through MEGF10 and MERTK pathways. *Nature* **504**, 394–400 (2013).

69. Vainchtein, I. D. *et al.* Astrocyte-derived interleukin-33 promotes microglial synapse engulfment and neural circuit development. *Science* **359**, 1269–1273 (2018).

70. Li, T. *et al.* A splicing isoform of GPR56 mediates microglial synaptic refinement via phosphatidylserine binding. *The EMBO Journal* **39**, e104136 (2020).

71. Scott-Hewitt, Nicole, et al. "Local externalization of phosphatidylserine mediates developmental synaptic pruning by microglia." The EMBO journal 39.16 (2020): e105380.

72. Deng, H., Chen, G., Yang, W. & Yang, J. J. Predicting calcium-binding sites in proteins—A graph theory and geometry approach. *Proteins: Structure, Function, and Bioinformatics* **64**, 34–42 (2006).

73. Rigden, D. J. & Galperin, M. Y. The DxDxDG Motif for Calcium Binding: Multiple Structural Contexts and Implications for Evolution. *Journal of Molecular Biology* **343**, 971–984 (2004).

74. Park, J. *et al.* Microglial MERTK eliminates phosphatidylserine-displaying inhibitory post-synapses. *The EMBO Journal* **40**, e107121 (2021).

75. Catterall, W. A. & Few, A. P. Calcium Channel Regulation and Presynaptic Plasticity. *Neuron* **59**, 882–901 (2008).

76. Nanou, E. & Catterall, W. A. Calcium Channels, Synaptic Plasticity, and Neuropsychiatric Disease. *Neuron* **98**, 466–481 (2018).

77. Dani, J. W., Chernjavsky, A. & Smith, S. J. Neuronal activity triggers calcium waves in hippocampal astrocyte networks. *Neuron* **8**, 429–440 (1992).

78. Chattopadhyay, N. *et al.* Extracellular calcium-sensing receptor in rat oligodendrocytes: Expression and potential role in regulation of cellular proliferation and an outward K+ channel. *Glia* **24**, 449–458 (1998).

79. Egelman, D. M. & Read Montague, P. Calcium Dynamics in the Extracellular Space of Mammalian Neural Tissue. *Biophysical Journal* **76**, 1856–1867 (1999).

80. Rusakov, D. A., Harrison, E. & Stewart, M. G. Synapses in hippocampus occupy only 1–2% of cell membranes and are spaced less than half-micron apart: a quantitative ultrastructural analysis with discussion of physiological implications. *Neuropharmacology* **37**, 513–521 (1998).

81. Jones, B. L. & Smith, S. M. Calcium-Sensing Receptor: A Key Target for Extracellular Calcium Signaling in Neurons. *Frontiers in Physiology* **7**, (2016).

82. Neniskyte, U. et al. Phospholipid scramblase Xkr8 is required for developmental axon pruning via phosphatidylserine exposure. The EMBO Journal e111790 (2023).

6. Acknowledgements

These five years have passed like a fleeting moment. Finally, I am graduating with an emotion, a joy and a hint of sadness. I am happy about the new life that awaits me, but also saddened to leave this familiar and cozy environment. I am very grateful for every lovely and respectable person I have met and who has helped me during these five years.

I want to express my special gratitude to the following individuals: Morimoto-san, who helped me with my research on membrane proteins; Kosako Sensei, who consistently assisted me in my experiments; Kimura Sensei, a kind and patient teacher who provided valuable guidance on liposome experiments; Ryo Sensei, who help me in conducting experiments related to membrane tension, and Abe Sensei, a very cool and kind person, who helped me analyze protein structures.

Among all, I want to express my special gratitude to my supervisor. My doctoral supervisor, Professor Suzuki (Suzuki Sensei). I am deeply thankful for the privilege of encountering such an amiable and respectable mentor in my life. In research, he is meticulous and cautious in his guidance, while in life, he is a kind and gentle person. I still remember when I joined Suzuki Lab at the beginning, Suzuki Sensei asked me a question, 'Do you know what GFP is?' At that time, I did not provide the correct answer. I felt ashamed that my three years of master's education could not reach the expected heights even though my previous boss did a lot for me. However, it was under such circumstances that Suzuki sensei patiently taught me how to conduct experiments, how to think, and how to become a competent researcher.

Research is never smooth sailing, and failures are a common aspect of a researcher’s journey. I started with my project: the purification of Xkr4, a project that consumed a significant part of my doctoral course. During those initial three years, experiments were repeatedly not going well, and I spent much of my time struggling in the failures, and started to doubt myself, my abilities, my dedication, and whether I was truly cut out for research field. Every time I found myself in this painful state of uncertainty, Suzuki Sensei would inspire me with his personal examples. He reminded me to view experimental results positively and that experimental failures are not to be feared. What matters is how to figure out the reasons behind these failures. Suzuki sensei often said that the experiment is kind of a process: step by step. Only by taking each step well, we can progress further. This is an important lesson I have learned, and I hope to carry this spirit forward in my future research career.

I want to express my gratitude to Maruoka-sensei for the help and care provided. Even though I have often troubled Maruoka-sensei with various minor issues, he has always responded with kindness and

patience, assisting me throughout. Thanks Shimomura-san for sharing the interesting things of Japan and a lot of help.

I am also thankful to every member of Suzuki Laboratory for your kind and help (Motani-sensei, Uchida-san, Noguchi-san, Matsui-san, Yamato-san, Niu Han, Suh-san, Ann-san, Erin-san, Dou-san, Shaan-san, Tadachi-san, Tachibara-san, Ishikawa Misato-san, Ishikawa Yukie-san, Pepe-san, Murakoso-san, Fujimoto-san, and Mori-san, Ohara-san, Mishiro-san, Katani-san). During my five years as a doctoral student, although it is just one-sixth of my life, it has been a significant period. I am honored to be a part of Suzuki Lab, a warm family. Hope this big family continues to thrive.

Lastly, I would like to express my gratitude to my parents and all my family. When I decided to come to Japan, they may not have fully agreed with my choice to go far, but they wholeheartedly supported my decision. There is an ancient Chinese saying, ' Whilst my parents are, I will never be far'. During my five years in Japan, I may not have been able to provide much care for them, but instead, they silently supported me, understood, and encouraged me, so that I could fully dedicate myself to my work. I am deeply grateful for their understanding and what they did always!

This thesis is based on material in the following scholarly papers.

Authors: Zhang Panpan, Maruoka Masahiro, Suzuki Ryo, Katani Hikaru, Dou Yu, Packwood Daniel. M, Kosako Hidetaka, Tanaka Motomu, Suzuki Jun.

Title: Extracellular calcium functions as a molecular glue for transmembrane helices to activate the scramblase Xkr4

Name of journal: Nature Communications.

DOI: 14, 5592.

Published date: 11 Sep 2023

Authors: Maruoka Masahiro, Zhang Panpan, Mori Hiromi, Imanishi Eiichi, Packwood Daniel. M, Kosako Hidetaka, Suzuki Jun.

Title: Caspase cleavage releases a nuclear protein fragment that stimulates phospholipid scrambling

at the plasma membrane

Name of journal: Molecular cell.

vol., no: 168.

page: 132-136.

Published date: In Apr, 2021.

Authors: Maruoka Masahiro, Zhang Panpan, Suzuki Jun.

Title: 不要細胞における“eat-me”シグナルの露出に関与する DNA 修復タンパク質 XRCC4 の新たな役割

Name of journal: 実験医学.

vol., no., page-page: 39/14　2021 年 9 月号

Published date: In Sep, 2021